New constraints on Eocene extension within the Canadian Cordillera and identification of Phanerozoic protoliths for footwall gneisses of the Okanagan Valley shear zone

Sarah R. Brown[1,2,*], H. Daniel Gibson[1], Graham D.M. Andrews[2], Derek J. Thorkelson[1], Daniel D. Marshall[1], Jeff D. Vervoort[3], and Nicole Rayner[4]
[1]DEPARTMENT OF EARTH SCIENCES, SIMON FRASER UNIVERSITY, 8888 UNIVERSITY DRIVE, BURNABY, BRITISH COLUMBIA V5A 1S6, CANADA
[2]EARTH RESEARCH INSTITUTE, UNIVERSITY OF CALIFORNIA–SANTA BARBARA, SANTA BARBARA, CALIFORNIA 93106, USA
[3]SCHOOL OF ENVIRONMENTAL AND EARTH SCIENCES, WASHINGTON STATE UNIVERSITY, PULLMAN, WASHINGTON 99164, USA
[4]GEOLOGICAL SURVEY OF CANADA, 601 BOOTH STREET, OTTAWA, ONTARIO K1A 0E8, CANADA

ABSTRACT

The Okanagan Valley shear zone delineates the SW margin of the Shuswap metamorphic complex, the largest core complex within the North American Cordillera. The Okanagan Valley shear zone is a major Eocene extensional fault zone that facilitated exhumation of the southern Shuswap metamorphic complex during the orogenic collapse of the SE Canadian Cordillera when convergence at the western margin of North America switched from transpression to transtension. This study documents the petrology, structure, and age of the Okanagan gneiss, the main lithology within the footwall of the Okanagan Valley shear zone, and constrains its history from protolith to exhumed shear zone. The Okanagan gneiss is an ~1.5-km-thick, west-dipping panel composed of intercalated orthogneiss and paragneiss in which intense ductile deformation of the Okanagan Valley shear zone is recorded. New U-Pb zircon ages from the gneiss and crosscutting intrusions constrain the development of the Okanagan gneiss to the Eocene, contemporaneous with widespread extension, intense deformation, high-grade metamorphism, and anatexis in the southern Canadian Cordillera. Thermobarometric data from the paragneiss domain indicate Eocene exhumation from between 17 and 23 km depth, which implies 64–89 km of WNW-directed horizontal extension based on an original shear zone angle of ~15°.

Neither the Okanagan gneiss nor its protolith represents exhumed Proterozoic North American cratonic basement as previously postulated. New U-Pb data demonstrate that the protolith for the gneiss is Phanerozoic, consisting of Mesozoic intrusions emplaced within a late Paleozoic–Mesozoic layered sequence of sedimentary rocks.

LITHOSPHERE; v. 4; no. 4; p. 354–377; GSA Data Repository Item 2012214. | Published online 4 June 2012. doi: 10.1130/L199.1

INTRODUCTION

This contribution focuses on the footwall domain of the Okanagan Valley shear zone, which is characterized by a >1-km-thick ductile shear zone that was in part overprinted by brittle deformation as the footwall was progressively exhumed during Eocene extension. A single discrete, unambiguous fault surface cannot be identified in most areas, where high-grade footwall gneisses are juxtaposed against low-grade to nonmetamorphosed hanging-wall lithologies, and given the predominance of ductile fabrics in the gneiss, we prefer to break from previous studies that hitherto have referred to the Okanagan Valley fault; we define the Okanagan Valley shear zone to include both ductile and brittle shear zones.

In the southern Canadian Cordillera, the Okanagan Valley shear zone was recognized as a major Eocene extensional fault with as much as 90 km of horizontal displacement (Tempelman-Kluit and Parkinson, 1986). More regionally, the Okanagan Valley shear zone is interpreted to represent the southern and central parts of a 450-km-long, en echelon fault system, the Okanagan Valley fault system of Johnson and Brown (1996), which delineates the western margin of the Shuswap metamorphic complex (Leech et al., 1963, p. 26; Wheeler, 1965; Okulitch, 1984). The Shuswap metamorphic complex is the largest metamorphic core complex in North America (Coney, 1980), where high-grade crystalline rocks exhumed from midcrustal levels in the Eocene (Parrish et al., 1988; Fig. 1) are exposed over an area of >40,000 km^2.

The Okanagan Valley shear zone and Okanagan gneiss are important tectonic and lithostratigraphic features with broad implications for understanding crustal evolution in the southern Canadian Cordillera. To this end, two outstanding issues related to the Okanagan Valley shear zone are addressed in this study: (1) the magnitude of extension across the Okanagan Valley shear zone and the way in which it may vary along strike, and (2) the age of the protolith and development of the Okanagan gneiss (Tempelman-Kluit, 1989), alternatively known as the Vaseaux Formation (sic Bostock, 1941; Armstrong et al., 1991) within the footwall of the Okanagan Valley shear zone.

How much extension did the Okanagan Valley shear zone accommodate? Several studies have focused along strike of the Okanagan Valley shear zone to the north (Fig. 1; Kelowna—Bardoux, 1993; Vernon—Glombick et al., 2006a; Shuswap Lake—Johnson, 2006) and south (Okanogan Dome—Kruckenberg et al., 2008). Studies to the north differ on the amount of extension across, and therefore the importance of, the Okanagan Valley shear zone system. Differences in the age and deformation of the gneisses, and apparent lateral continuity of upper-plate stratigraphy

*E-mail: srbrown19@gmail.com.

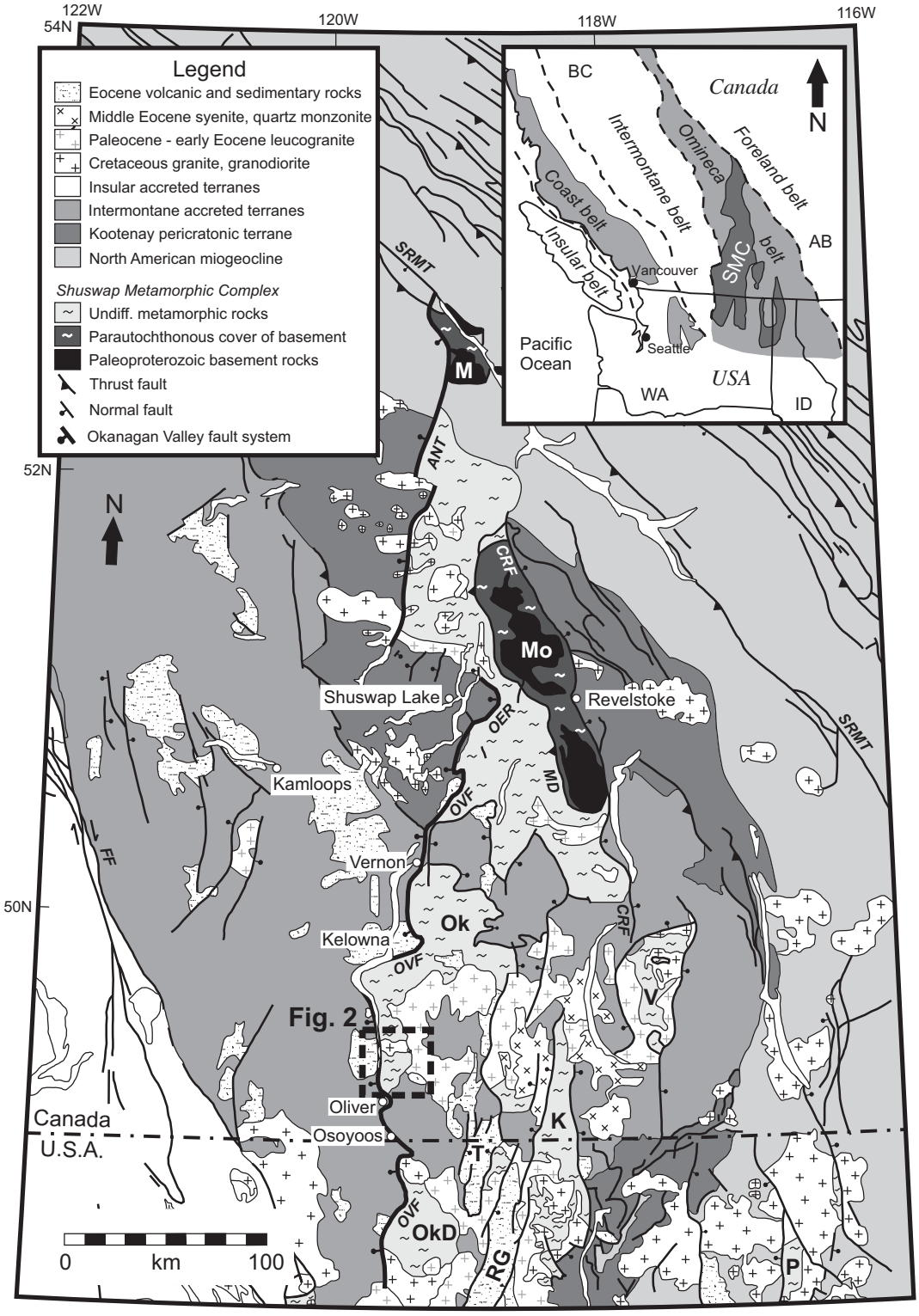

Figure 1. Simplified geological map of the Shuswap metamorphic complex (SMC) in British Columbia and northern Washington State. Paleoproterozoic, ancestral North American basement is exposed in the Monashee (Mo) and Malton (M) gneiss domes in the northern Shuswap metamorphic complex. Figure is adapted from Johnson (2006) and Kruckenberg et al. (2008). Other abbreviations: ANT—Adams Lake–North Thompson fault; CRF—Columbia River fault; FF—Fraser fault; K—Kettle River–Grand Forks Dome; MD—Monashee décollement; OER—Okanagan-Eagle River; Ok—Okanagan complex; OkD—Okanogan Dome; OVF—Okanagan Valley fault; P—Priest River complex; RG—Republic graben; SRMT—Southern Rocky Mountain trench; T—Toroda Creek graben; V—Valhalla Dome. Inset: Simplified map of the southern Canadian Cordillera showing morphogeologic belts and the outline of the Shuswap metamorphic complex (dark gray).

in the Vernon area led Glombick et al. (2006a) to conclude that, in this region, the horizontal extension across the Okanagan Valley shear zone was 0–12 km. This is significantly less than that proposed to the north and south along the Okanagan Valley shear zone system (30–90 km) by Tempelman-Kluit and Parkinson (1986), Parrish et al. (1988), Bardoux (1993), and Johnson and Brown (1996). Although the entire Okanagan Valley shear zone system need not exhibit consistent horizontal extension along its strike, the 80–90 km differences in interpreted extension, in the presence of very similar footwall and hanging-wall geology along strike, need to be reconciled. Constraining extension across the Okanagan Valley shear zone in the southern Okanagan Valley is therefore an important theme, and our results have important regional implications for assessing these opposing estimates.

Does part of the Okanagan gneiss represent a piece of ancestral North American basement? Despite the fact that the southern Okanagan Valley is the reference location for the Okanagan Valley shear zone and the Okanagan gneiss (Tempelman-Kluit, 1989), very little is known in detail about the lithologies and their geochronology, for example: (1) the age of the protolith(s); (2) the proportion of paragneiss to orthogneiss; and (3) the age and duration of gneiss formation, including metamorphism and exhumation history. In their pioneering study of the age and isotopic characteristics of crystalline rocks in the Shuswap metamorphic complex, Armstrong et al. (1991) concluded that part of the Okanagan gneiss represented a segment of Proterozoic North American basement exhumed in the Eocene, correlative with Paleoproterozoic gneiss domes in the Monashee complex (Fig. 1; Armstrong et al., 1991; Parkinson, 1991; Crowley, 1999). This interpretation placed the Okanagan gneiss as the most westerly exposure of Precambrian basement gneiss in the North American Cordillera, and it has been an important influence for interpreting crustal seismic profiles (e.g., Cook et al., 1992; Cook, 1995) and establishing estimates of total shortening and extension within the Cordillera (e.g., Johnson and Brown, 1996). Many studies continue to depict the Okanagan gneiss as Early Proterozoic North American cratonic basement (e.g., Wheeler and McFeely, 1991; Bardoux and Mareschal, 1994; Glombick et al., 2006b; Cui and Erdmer, 2009). However, there is a paucity of supporting data for this interpretation, including a lack of modern geochronological data.

This paper reports the results of our study of the petrology, structure, and geochronology of the Okanagan gneiss, which is restricted to the footwall of the Okanagan Valley shear zone. These results provide insight into the ages of the protolith, igneous intrusions, shear zone development, and associated metamorphic recrystallization. These new data provide an opportunity for future investigation of core complex formation, gneiss dome emplacement, midcrustal flow, and the evolution of postorogenic extensional systems.

Geological Context

The Shuswap metamorphic complex is a region of thinned and exhumed, crystalline, midcrustal rocks within the Omineca belt where sillimanite-bearing, amphibolite- and granulite-facies gneisses and schists, and assorted intermediate and felsic intrusions, are exposed in a series of gneiss domes (Fig. 1). The Okanagan gneiss is located along the western margin of the Shuswap metamorphic complex and is interpreted to have been exhumed from the midcrust (Ewing, 1980) along low-angle detachment faults (Tempelman-Kluit and Parkinson, 1986; Parrish et al., 1988), including the Okanagan Valley shear zone, during Eocene transtension following tectonic thickening during the Jurassic–Paleocene Cordilleran orogeny (Okulitch, 1984; Tempelman-Kluit and Parkinson, 1986; Kruckenberg et al., 2008; Gervais and Brown, 2011).

The Okanagan gneiss (Tempelman-Kluit, 1989) is a sequence of upper-amphibolite-facies paragneiss, orthogneiss, and migmatite intruded by granitic and pegmatite sheets. These units are exposed in a semicontinuous belt along the eastern flank of the Okanagan Valley in southern British Columbia and northern Washington State (Fig. 1). The high-grade gneisses within the footwall of the Okanagan Valley shear zone are juxtaposed against nonmetamorphosed volcanic and volcaniclastic rocks, and a sequence of relatively low-metamorphic-grade metasedimentary and metavolcanic rocks intruded by granitic plutons (Fig. 2; Tempelman-Kluit, 1989). On the basis of the contrast in metamorphic grade and cooling ages observed across the Okanagan Valley, and the strong noncoaxial deformation recorded within the gneisses, a significant 10° to 30° west-dipping extensional shear zone was proposed by Tempelman-Kluit and Parkinson (1986). The shear zone is ~1.5 km thick and grades structurally upward from mylonitic amphibolite-facies gneiss to cataclasite where the shear zone is bounded by an upper brittle detachment surface.

The Okanagan gneiss is one of several gneissic culminations within the Shuswap metamorphic complex (Fig. 1), including the Okanogan Dome (Kruckenberg et al., 2008), Valhalla (Gordon et al., 2008) and Passmore Domes, Aberdeen gneiss complex (Glombick et al., 2006a, 2006b), Thor-Odin dome (Hinchey and Carr, 2006; Hinchey et al., 2006), and Grand Forks–Kettle River complex (Laberge and Pattison, 2007). Several of these studies have determined that high-temperature metamorphism, anatexis, and associated magma emplacement were coeval with extension and exhumation along adjacent detachments shear zones (e.g., Teyssier et al., 2005; Gordon et al., 2008). All these neighboring gneiss complexes record metamorphism and exhumation in the Paleocene to early Eocene, for example, migmatization in the Okanogan Dome at 61–49 Ma (Kruckenberg et al., 2008).

GEOLOGY OF THE OKANAGAN VALLEY SHEAR ZONE

The footwall of the Okanagan Valley shear zone (i.e., the lower plate) is composed of weakly to nondeformed granitoid plutons that grade upward into the base of the Okanagan Valley shear zone, where they become progressively more foliated and gneissic. The Okanagan Valley shear zone (Fig. 2) is composed of three vertically gradational lithodemic domains. In ascending structural order in the crust, they are: (1) weakly to moderately foliated felsic plutonic rocks that are gradational with nondeformed rocks in the footwall; (2) mylonitized, moderately to intensely deformed orthogneiss and paragneiss pervasively intruded by felsic sheets; and (3) hydrothermally altered ultramylonite, cataclasite, and breccia. The hanging wall (i.e., the upper plate) is composed of subgreenschist- to greenschist-facies marine metasedimentary rocks consisting predominantly of phyllite and schist (e.g., the Kobau Group; Okulitch, 1973), felsic plutons, and nonmetamorphosed terrestrial Eocene volcanic, volcaniclastic, and sedimentary rocks (Church, 1973).

In keeping with interpretations of previous workers (e.g., Parkinson, 1985; Tempelman-Kluit and Parkinson, 1986; Bardoux, 1993), the Okanagan Valley shear zone is comparable to typical detachments bounding many metamorphic core complexes (e.g., Davis, 1983; Davis and Lister, 1988; Reynolds and Lister, 1990), through: (1) the juxtaposition of strongly deformed crystalline rocks against nonmetamorphosed upper-plate rocks, (2) gradual grain-size reduction of gneiss to mylonite to cataclasite toward the upper levels of the fault zone, and (3) the brittle overprinting of earlier and deeper-formed ductile fabrics. It is clear that the Okanagan gneiss and footwall were exhumed along the Okanagan Valley shear zone such that the gneiss was progressively overprinted by mylonitic and cataclastic fabrics characteristic of medial and shallow crustal levels, respectively.

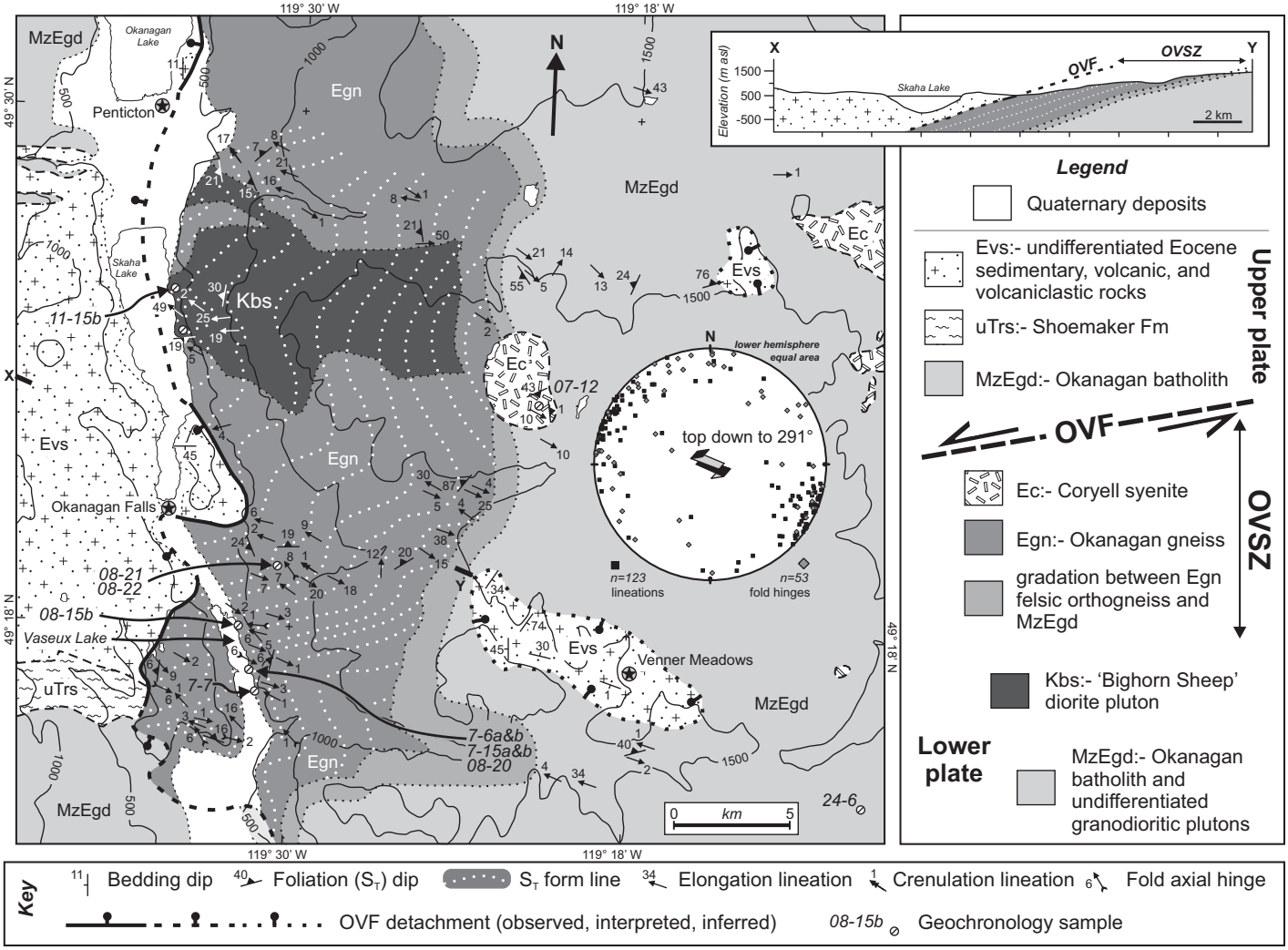

Figure 2. Simplified geologic map of the southern Okanagan Valley south of Penticton, British Columbia, adapted from Tempelman-Kluit (1989), showing the Okanagan Valley shear zone (OVSZ), Okanagan Valley fault (OVF), and sample locations. Okanagan gneiss transposition foliation (ST) form lines indicate long-wavelength warping of the shear zone. Cross-section X–Y depicts the width of the ~18°W-dipping Okanagan Valley shear zone and the way in which it is bounded on the upper and western margin by the Okanagan Valley fault; extension is top-to-the-west. Inset: lower-hemisphere equal-area projection of lineations (mean trend ~291°) and fold axes in the Okanagan gneiss. VL—Vaseux Lake (adjacent to 08-15b); asl—above sea level.

Plutonic Rocks of the Okanagan Valley Shear Zone Footwall

Calc-alkaline and I-type plutonic rocks, chiefly granodiorite and diorite, are abundant throughout the southern Okanagan area and adjacent regions, and they have typically been assigned to the composite Jurassic–Cretaceous Okanagan batholith, and to a lesser degree, the Middle Jurassic Nelson suite (Tempelman-Kluit, 1989; Woodsworth et al., 1991). Assignment of plutonic rocks to the Okanagan batholith was based primarily on similarity in appearance and composition, as there were very little geochemical and geochronological data available. The majority of previous age determinations for the batholith were derived from K-Ar mica and hornblende ages that range from 58 to 50 Ma (Breitsprecher and Mortensen, 2004), but this only reflects the time the plutons were exhumed and cooled through ~300 °C (Harrison et al., 1985), not true crystallization ages. The Okanagan batholith is likely a composite body that was assembled from Jurassic to Cretaceous time coincident with voluminous calc-alkaline magmatism throughout much of the western margin of North America (Armstrong, 1988; Woodsworth et al., 1991; Carr, 1992). Contemporaneous Eocene alkaline (e.g., Coryell syenite; Tempelman-Kluit, 1989; Ghosh, 1995a) and S-type leucogranite laccoliths (e.g., ca. 60–56 Ma Ladybird granite—Carr, 1992; Ghosh, 1995a; Vanderhaeghe et al., 1999; Hinchey and Carr, 2006; Colville batholith—Holder and McCarley Holder, 1988) are also locally abundant and rarely differentiated within the batholith.

Massive, hornblende-phyric (±biotite) granodiorite (unit MzEgd, Fig. 2) is the dominant lithology in the lower plate of the Okanagan Valley shear zone, structurally below a carapace of the Okanagan gneiss; small diorite plutons (e.g., the Bighorn Sheep pluton, unit Kbs in Fig. 2; "unit Eg" of Tempelman-Kluit, 1989) occur within the larger granodiorite mass. Granodiorite and diorite are both pervasively intruded by crosscutting pre- and post-tectonic granite, and granitic pegmatite and aplite sheets. Nonfoliated granodiorite grades structurally upward from east to west over 1–2 km into progressively more foliated granodiorite (Fig. 3A), augen gneiss (Fig. 3B), and eventually mylonitized felsic orthogneiss within the

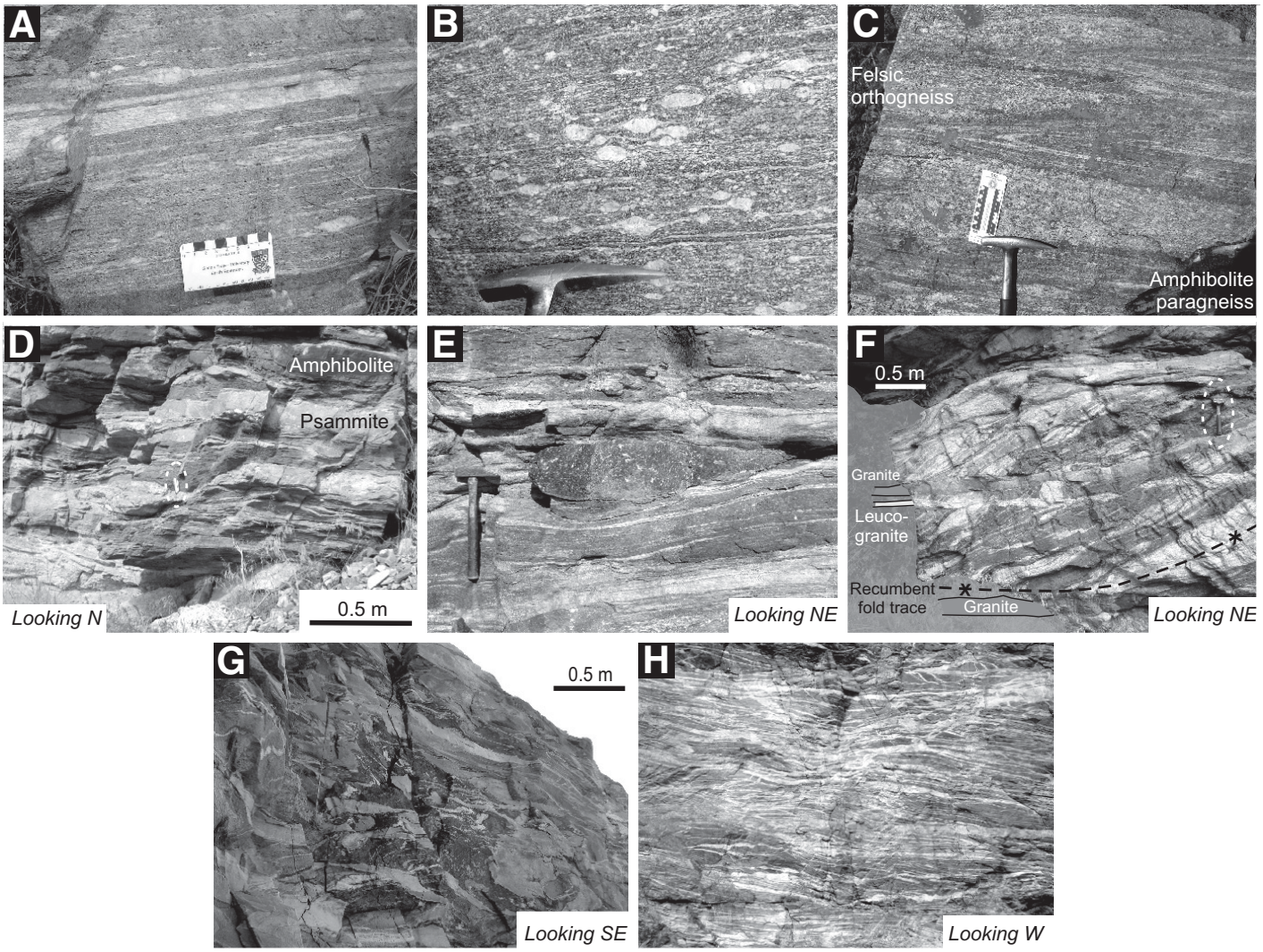

Figure 3. (A) Strongly foliated granodiorite in the footwall of the Okanagan Valley shear zone. (B) Felsic augen gneiss developed within the transition from footwall to Okanagan Valley shear zone. (C) Folded and intercalated felsic orthogneiss and amphibolite paragneiss. (D) Transposed lithological layering within the amphibolite paragneiss. Psammitic layers are resistive, whereas pelitic and amphibolitic layers are recessive. Pen knife (~8 cm) is shown for scale (circled). (E) Intrafolial ultramafic boudin within the paragneiss. (F) Recumbently folded gneiss at the base of the paragneiss domain, crosscut by attenuated subhorizontal granite and leucogranite sheets. All the rocks exhibit a penetrative, subhorizontal fabric. Rock hammer (~30 cm) is shown for scale (circled). (G) Folded paleosome (dark center) surrounded by melanosome, and both pervasively intruded by, and subsequently deformed with, leucosome and felsic sheets. (H) A network of leucosome and leucogranitic sheets (i.e., net structure sensu Sawyer, 2008), with a dominant subhorizontal fabric, intruded into the paleosome. Net structure is characteristic of metatexite, where the degree of partial melting within the migmatite is ≤~25%.

Okanagan Valley shear zone. The relationship is interpreted as a preserved strain gradient within the lower plate that delineates the lower boundary of the Okanagan Valley shear zone. The transition between deformed and nondeformed plutonic rocks is difficult to trace due to poor exposure, subtle magmatic and tectonic fabrics, and the gradational nature of the strain gradient over >1 km. In the Kelowna area (Fig. 1), the transition from granodiorite to orthogneiss commonly coincides with the occurrence of abundant pegmatite and evidence of migmatization (Bardoux, 1993).

Locally, the margin of the shear zone is sharply defined where variably foliated granodiorite or diorite is interlayered with mafic orthogneiss and paragneiss. Within this mixed region, boudins and screens of granodiorite and granodioritic orthogneiss are intercalated, transposed, and interfolded with boudins and screens of mafic orthogneiss. The irregularity of this contact is at least partly tectonic in origin, but deformation of an originally irregular intrusive contact also remains possible.

The Okanagan Gneiss

The Okanagan gneiss is a distinctive sequence of layered amphibolite gneiss with localized zones of migmatite and ubiquitous felsic and pegmatitic sheet-like intrusions, plastically deformed within the Okanagan Valley shear zone.

Three lithological domains can be distinguished within the Okanagan gneiss (Table 1), in decreasing volume: ubiquitous felsic orthogneiss, a ubiquitous mixed paragneiss and mafic orthogneiss domain, and a localized migmatite domain, all of which are overprinted by a penetrative shear

TABLE 1. LITHOLOGICAL UNITS WITHIN THE OKANAGAN GNEISS

Domain	Lithologies	Dominant fabric	Inferred protolith
Orthogneiss	Dioritic and granodioritic orthogneiss, augen gneiss, crosscutting granitic pegmatite and granite sheets.	Transposed gneissic foliation: alternating, millimeter- to centimeter-scale, hornblende-rich and -poor folia.	Okanagan batholith (Okanagan Valley shear zone footwall).
Paragneiss with amphibolite sheets	Paragneiss with lesser metapelite, psammite, marble, and ultramafic boudins; crosscutting granitic pegmatite and granite sheets.	Transposed lithological layering.	Marine volcano-sedimentary succession (graywacke, pelite, psammite, and carbonate) intruded by (ultra)-mafic sheets.
Migmatite	Diatexite. Granoblastic amphibolite melanosome pervasively intruded by leucosome, granitic pegmatite, and granite sheets.	Relic gneiss foliation.	Amphibolite paragneiss.

zone fabric. The gneiss is intimately associated with the Okanagan Valley shear zone and does not occur independently of it; the spatial distributions of the different lithological domains are complex and are not yet resolved (Fig. 2). The Okanagan gneiss and underlying footwall are crosscut by a multitude of peraluminous, garnetiferous, S-type granite sheets, many of which postdate some or all folding and transposition within the gneiss.

Felsic Orthogneiss

The felsic orthogneiss grades structurally downward into foliated and eventually nonfoliated diorite and granodiorite within the footwall. The orthogneiss is typically gray and variably foliated (W-dipping), locally with layers of augen gneiss (Fig. 3B). Contact relationships with the paragneiss are uncertain, although they are, at least locally, interfolded (e.g., Fig. 3C).

Paragneiss Domain

The paragneiss domain is a heterogeneous package of decimeter- to meter-thick, laterally discontinuous, folded and transposed layers (e.g., Fig. 3D) of: (1) medium to coarse, equicrystalline, mesocratic, finely banded K-feldspar–hornblende–quartz (±garnet, ±sillimanite) amphibolite gneiss; (2) coarse psammite; (3) garnetiferous biotite schist (metapelite); (4) melanocratic hornblende-garnet and hornblende-clinozoisite ultramafic orthogneiss boudins (Fig. 3E); and (5) rare calc-silicate marble. Layers are interfolded, crosscut by granite and granitic pegmatite sheets (Fig. 3F), and have a penetrative shear zone fabric.

The presence of quartz-rich sandstones, graywackes, pelite, and carbonate protoliths suggests a marine depositional setting. The protolith of the mesocratic amphibolite gneiss layers is less certain; we infer it to be a sedimentary or volcaniclastic deposit, perhaps a graywacke, based on mineralogy, association with other sedimentary layers, and thickness.

Thermobarometry

Numerous samples were examined for suitable mineral assemblages for pressure and temperature (*P-T*) determinations within the Okanagan gneiss. Due to bulk composition or retrograde alteration (cf. Bardoux, 1993), the only sample deemed representative of preserved peak metamorphic conditions was sample 08-12, from a garnetiferous schist layer within the paragneiss domain.

We used electron microprobe analyses (Appendix A; GSA Data Repository DR1[1]) of anhedral almandine porphyroblasts with biotite, plagioclase, and muscovite inclusions, and the surrounding biotite-muscovite-plagioclase matrix (Fig. 4A) to assess the degree of compositional equilibrium within the sample. FeO, MnO, and MgO profiles across almandine porphyroblasts are uniformly flat except where ≤1-mm-thick rims featuring 2 wt% FeO enrichment and MnO depletion are present (Table 2; Fig. 4B, inset). These minor differences in the core and rim garnet compositions suggest minor retrograde re-equilibration of the garnet, with the core representing equilibration at peak or near-peak metamorphic conditions. Biotite, muscovite, and plagioclase compositions are consistent (≤0.5 wt% difference) between the matrix and inclusions within garnet porphyroblasts (Table 2), indicating that the porphyroblasts and matrix are in equilibrium. Assuming complete resetting, minimum *P-T* estimates can be obtained; in contrast, if they are not reset, then peak or near-peak *P-T* conditions may be derived.

Mineral composition data were applied to the garnet-biotite thermometer of Ferry and Spear (1978), and the garnet-muscovite-annite-plagioclase barometer of Hoisch (1990, 1991) using the winTWQ (v. 2.3; Berman, 2007) database and model of Berman (1991). The activity models used were those of Berman and Aranovich (1996) for garnet, Berman et al. (2007) for biotite, and Furhman and Lindsley (1988) for plagioclase. *P-T* results indicate that the garnet cores, rims, and the matrix equilibrated at 670 °C ± 50 °C and ~6.2 ± 1.0 kbar (Fig. 4B), equivalent to ~20 km depth.

The *P-T* data are consistent with metamorphism to upper amphibolite facies and sillimanite grade (Fig. 4B), at or beyond the wet granite solidus; these interpretations are supported by the dominance of amphibolite in the Okanagan gneiss, the reported presence of sillimanite (Bardoux, 1993), and the presence of migmatite (see following). It is possible that all the mineral compositions have been reset at different times; however, we deem that very unlikely because the derived *P-T* data are fairly consistent from garnet core to rim, and consistent with the geological models, metamorphic conditions, and *P-T* histories for similar units elsewhere in the southern Shuswap metamorphic complex (e.g., Bardoux, 1993; Laberge and Pattison, 2007).

Migmatite

The migmatite domain is small and restricted to the area at the southern end of Vaseux Lake (Fig. 2). Migmatite terminology used is that of Sawyer (2008) and Sawyer et al. (2011). Rafts of paleosome (i.e., nonmelted amphibolite gneiss) are surrounded by medium to coarsely crystalline, granoblastic melanosome (Fig. 3G; hornblende–K-feldspar ± garnet), and both are pervasively intruded (Fig. 3H) by networks of pre- and syntectonic leucosome sheets and veins, stromatic leucosome veins, and granite pegmatite sheets, and individual, planar pre-, syn-, and post-tectonic granite dikes and sills. Felsic intrusions and leucosomes compose ≤60% of the total rock volume. Lithological layering and gneissic foliation are present and laterally continuous within the paleosome, and to a lesser degree the melanosome, and are similar to those in the Okanagan Valley shear zone as a whole.

We interpret this domain as a metatexite migmatite (Sawyer, 2008) based on (1) the network (i.e., "net-structure" sensu Sawyer, 2008) of

[1]GSA Data Repository Item 2012214, electron microprobe and U-Pb data, is available at www.geosociety.org/pubs/ft2012.htm, or on request from editing@geosociety.org, Documents Secretary, GSA, P.O. Box 9140, Boulder, CO 80301-9140, USA.

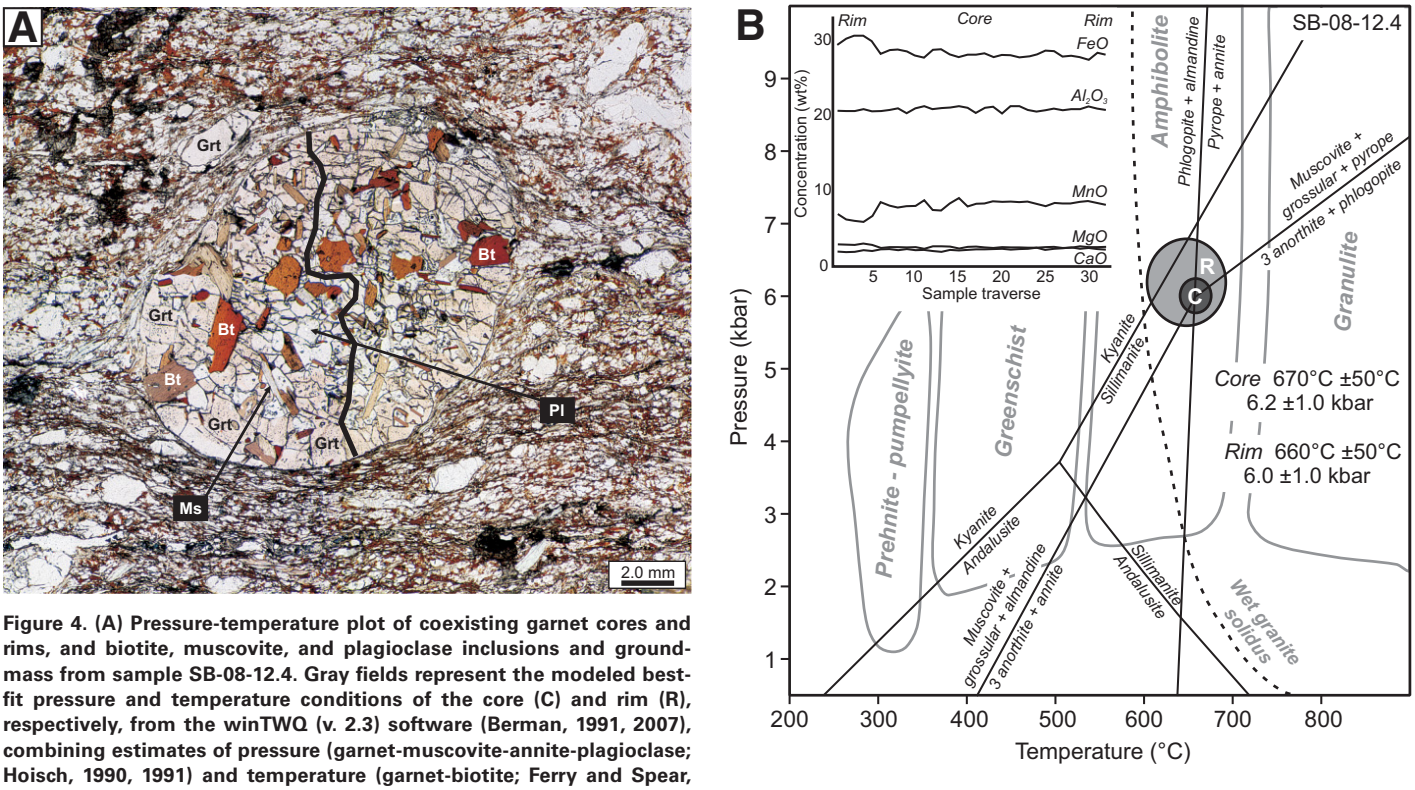

Figure 4. (A) Pressure-temperature plot of coexisting garnet cores and rims, and biotite, muscovite, and plagioclase inclusions and groundmass from sample SB-08-12.4. Gray fields represent the modeled best-fit pressure and temperature conditions of the core (C) and rim (R), respectively, from the winTWQ (v. 2.3) software (Berman, 1991, 2007), combining estimates of pressure (garnet-muscovite-annite-plagioclase; Hoisch, 1990, 1991) and temperature (garnet-biotite; Ferry and Spear, 1978). Wet granite solidus is after Winter (2010). (A, inset) Selected major-oxide concentrations along the traverse pathway show no significant change from rim to core to rim, suggesting little or no retrogression. (B) Photomicrograph (plane polars) of a biotite + plagioclase + muscovite inclusion–rich, anhedral garnet porphyroblast and traverse pathway (heavy black signature).

TABLE 2. REPRESENTATIVE ELECTRON MICROPROBE ANALYSES FOR GARNET, BIOTITE, MUSCOVITE, AND FELDSPAR IN SAMPLE SB-08-12.4

Analysis	Grt-core	Grt-rim	Bt-matrix	Bt-inclusions	Ms-matrix	Ms-inclusions	Feldspar
Na_2O (wt%)	0.01	0.01	0.12	0.14	0.45	0.50	7.72
MgO	2.58	2.96	8.58	8.15	0.76	0.90	0.00
Al_2O_3	21.24	21.02	18.37	19.11	34.35	34.11	24.67
SiO_2	36.38	36.33	35.51	35.67	46.00	46.34	60.74
K_2O			9.51	9.62	10.75	10.64	0.28
CaO	2.37	2.04	0.04	0.01	0.01	0.01	6.40
TiO_2	0.02	0.05	2.81	2.75	0.85	0.83	
Cr_2O_3	0.01	0.02	0.04	0.03	0.02	0.02	
MnO	8.57	6.50	0.37	0.35	0.02	0.04	0.01
FeO	28.50	30.68	20.23	19.72	1.25	1.54	0.09
F			0.28	0.22	0.05	0.08	
Cl			0.05	0.05	0.01	0.01	
Total	99.67	99.60	95.91	95.82	94.52	95.00	99.91
n	15	5	10	16	19	14	21

leucosome sheets (e.g., Fig. 3G) and synmigmatitic stromatic layering, (2) the continuity of original gneissic foliation (e.g., Kruckenberg and Whitney, 2011), and (3) the absence of pervasive in situ melt features. Folding of the paleosome, neosome, and felsic intrusions suggests syntectonic anatexis, similar to variably deformed metatexite and diatexite that occur together in the adjacent Okanogan Dome, Washington State (Fig. 1; Kruckenberg et al., 2008).

The relationship between the metatexite and the adjacent paragneiss and orthogneiss domains is unclear; however, the abundance of melanosome suggests a ferromagnesian-rich or pelitic protolith, perhaps an amphibolitic paragneiss. We have not determined the source of the leucosome sheets; that is, how much was produced within the exposed metatexite versus that intruded from a source elsewhere.

Ductile Deformation within the Okanagan Gneiss

Planar fabric elements. Planar fabric elements and folds within the Okanagan gneiss are ubiquitously (re-)folded, attenuated, and laterally discontinuous, forming boudins and rootless fold hinges. The dominant planar fabric element is a penetrative, composite transposition foliation (S_T) dipping 5°–30°W (median 15°W) (Fig. 2). S_T consists of two

parallel planar elements: alternating mafic (typically hornblende-rich) and felsic (typically hornblende-poor) layers that define a gneissic foliation (S_G) in the orthogneiss (Fig. 3B) and migmatite domains, and penetrative lithological layering in the paragneiss domain (Fig. 3C), similar to that identified in the Monashee gneiss dome (Fig. 1; Reesor and Moore, 1971). The lithologic layering and S_G, along with pegmatitic sheets that crosscut them, are deformed, transposed, and repeated by ubiquitous intrafolial centimeter- to decimeter-scale, isoclinal and recumbent folds with axial planes parallel to S_T.

Incipient development of S_T may have occurred during the widespread Mesozoic compression in the southern Canadian Cordillera that accompanied accretion of the Intermontane superterrane (e.g., Gibson et al., 2008). However, no definitively earlier fabrics have been found in the study area. A proto- to mylonitic fabric (herein referred to as S_M) overprints and is subparallel to S_T and the Okanagan Valley shear zone, is locally penetrative, and tends to become more intense (i.e., mylonite and ultramylonite) upward within the Okanagan Valley shear zone. For example, felsic sheets that crosscut S_T, and that have chilled margins, themselves exhibit a slightly oblique overprinting mylonitic fabric (S_M) (Fig. 5A). Based on these observations, we interpret S_M to have developed at a slightly younger time, as the footwall of the Okanagan Valley shear zone was being exhumed and experiencing lower ambient temperatures, which led to more partitioning of the shear zone strain into less competent, "softer" rheologies.

S_T and S_M are both warped by 10-m-scale to kilometer-scale, very open and upright, periclines (Fig. 2: S_T form lines) inferred to relate to synexhumation, buckle folding of the entire Okanagan Valley shear zone (Brown, 2010). This suggests that weak, coaxial plastic deformation throughout the Okanagan Valley shear zone immediately followed, or was contemporaneous with, mylonitization caused by noncoaxial strain along the Okanagan Valley shear zone.

Linear fabric elements and kinematic criteria. Linear fabric elements are mostly limited to an elongation lineation defined by alignment of hornblende laths and quartz rodding in orthogneiss and pre- and syntectonic intrusions, and by fold hinges of sheath folds (Fig. 5B). Where present, these lineations are typically downdip to S_T (shallowly to moderately plunging toward 291°; Fig. 2, inset). Kinematic criteria, including δ- and σ-mantled porphyroclasts (Fig. 5C), shear bands, C/S fabrics (Fig. 5D), and fold vergence patterns (Fig. 5E), record an extensional top-down-to-the-west-northwest shear sense that largely parallels the trend of the elongation lineation.

Structures now preserved within the Okanagan gneiss are interpreted to have resulted from progressive extensional general shear strain within the Okanagan Valley shear zone. Similar structural elements and kinematic criteria are observed in adjacent parts of the Okanagan Valley shear zone (e.g., Parkinson, 1985; Bardoux, 1993; Kruckenberg et al., 2008). Based on these relationships, we summarize: (1) Strongly noncoaxial plastic shear strain within the Okanagan Valley shear zone produced an elongation lineation, transposition fabric (S_T), and recumbent isoclines and sheath folds. (2) Progressive exhumation of the Okanagan Valley shear zone gradually overprinted S_T and intrusions in it with a penetrative proto- to mylonitic fabric (S_M; e.g., Fig. 5A). (3) During exhumation and mylonization, the Okanagan Valley shear zone was buckled into a series of periclines.

Upper Boundary of the Okanagan Valley Shear Zone

In the study area, there is typically a 20–40-m-thick, subhorizontal to gently west-dipping zone composed of mylonitic and cataclastic rocks

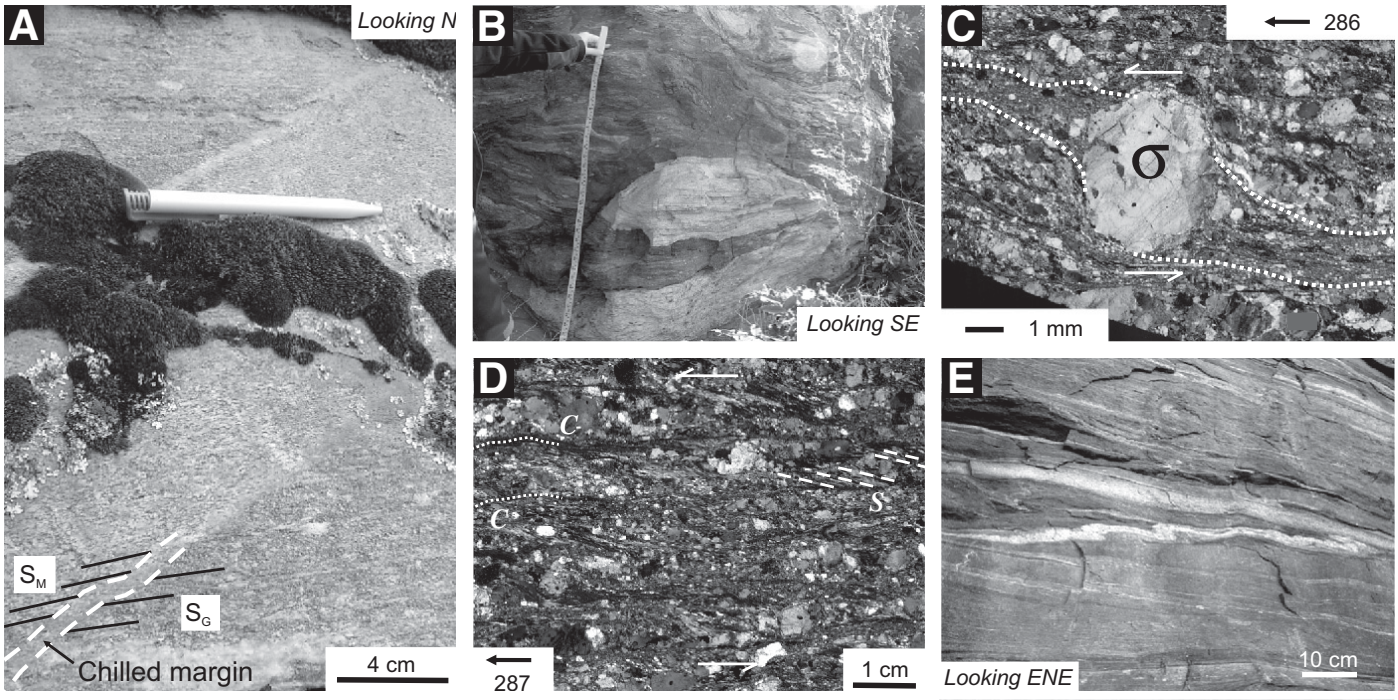

Figure 5. (A) Relative timing of fabric-forming events: a granite dike with chilled margins crosscutting the gneissic foliation (SG) at a high angle is, itself, overprinted by a protomylonitic fabric (SM) that is subparallel to SG. (B) "Eye structure" of pegmatite surrounded by amphibolite gneiss interpreted to be a sheath fold closure, viewed parallel to the elongation lineation (~290°). Measuring tape with 1 cm increments for scale. (C) Photomicrograph showing a σ-object quartz porphyroclast with top-to-the-west shear sense in orthogneiss. (D) Photomicrograph showing C/S fabric developed in amphibolite paragneiss; top-to-west shear sense. (E) Folded leucosome stromata in stromatic migmatite with top-to-west fold vergence.

forming the upper structural margin of the Okanagan Valley shear zone. This boundary separates metamorphosed, ductilely deformed, crystalline rocks of the footwall and the Okanagan Valley shear zone (e.g., the Okanagan gneiss) from nonmetamorphosed clastic rocks of the hanging wall (Fig. 2, inset). The Okanagan Valley shear zone grades progressively upward from protomylonitized orthogneiss, paragneiss, and migmatite into mylonitic gneiss, ultramylonite (Fig. 6A), chlorite breccia, and cataclastite. Ultramylonite layers are typically deformed by curvilinear, overturned folds (Fig. 6A); pseudotachylyte veins (≤1 mm thick) are present and are parallel to the ultramylonitic fabric (Fig. 6B). Rocks within the upper part of the fault zone, including the mylonite, and in the adjacent hanging wall, are strongly brecciated (Figs. 6C and 6D) and often silicified.

The Hanging Wall

Widespread Eocene extension is also manifested throughout the region west of the Okanagan Valley shear zone (e.g., Ewing, 1980, 1981) in the form of normal faults, graben (e.g., Fig Lake graben; Thorkelson, 1989), and horsts (e.g., Nicola horst; e.g., Cook et al., 1992). These extensional features are also found within the upper plate of the Okanagan Valley shear zone (described in the following), and are a consequence of brittle extensional deformation in the cold hanging wall during west-northwest–directed extensional shear on the Okanagan Valley shear zone.

Rocks in the hanging wall of the Okanagan Valley shear zone (Fig. 2) consist of zeolite to lower-greenschist-facies rocks of the Intermontane belt (Fig. 1 inset), including the Shoemaker Formation, that record predominantly Mesozoic cooling ages (Parrish et al., 1988). These are predominantly accreted Paleozoic to Early Jurassic metasedimentary and metavolcanic rocks of oceanic and juvenile oceanic-arc affinity that have been intruded multiple times by pre-Triassic through Middle Eocene plutons including the Okanagan batholith (Okulitch, 1979; Parkinson, 1985; Ghosh, 1995a). The Mesozoic hanging-wall rocks are overlain by Eocene nonmetamorphosed sedimentary, volcanic, and volcaniclastic rocks that were, in part, deposited into small supradetachment half graben above the Okanagan Valley shear zone (Mathews, 1981; McClaughry and Gaylord, 2005), including the 2300-m-thick succession in White Lake basin (Fig. 1; Church, 1973; McClaughry and Gaylord, 2005). Vitrinite reflectance data (Eyal et al., 2006) indicate that the present-day top of the White Lake basin succession was buried by ~3.5 km of material that eroded before the middle Miocene.

Middle Eocene (ca. 49 Ma; Breitsprecher and Mortensen, 2004) sedimentary and volcaniclastic rocks within the upper part of the White Lake basin (Skaha Formation) were being deposited at the same time during which the Okanagan gneiss was still at ~300 °C (~10 km depth), based on $^{40}Ar/^{39}Ar$ cooling ages for the Okanagan gneiss (e.g., Mathews, 1981; Armstrong et al., 1991). McClaughry and Gaylord (2005) reported that the Skaha Formation contains clasts of schist and mylonite that may have been derived from the Okanagan Valley shear zone. If correct, this finding would imply that parts of the Okanagan Valley shear zone were being exhumed and eroded during deposition of the Skaha Formation, and that exhumation at ca. 49 Ma was rapid.

Klippen

Supradetachment klippen composed of Eocene sedimentary, volcanic, and volcaniclastic rocks, identical to those in the western hanging wall of the Okanagan Valley shear zone, occur to the east of the Okanagan Valley (e.g., Venner Meadows, Fig. 2). Despite a lack of outcrop, the Okanagan Valley shear zone is identified beneath the klippe at Venner Meadows through drill cores that penetrate fault gouge, chlorite breccias, and mylonite, into the Okanagan gneiss (Morin, 1989). Scattered Eocene

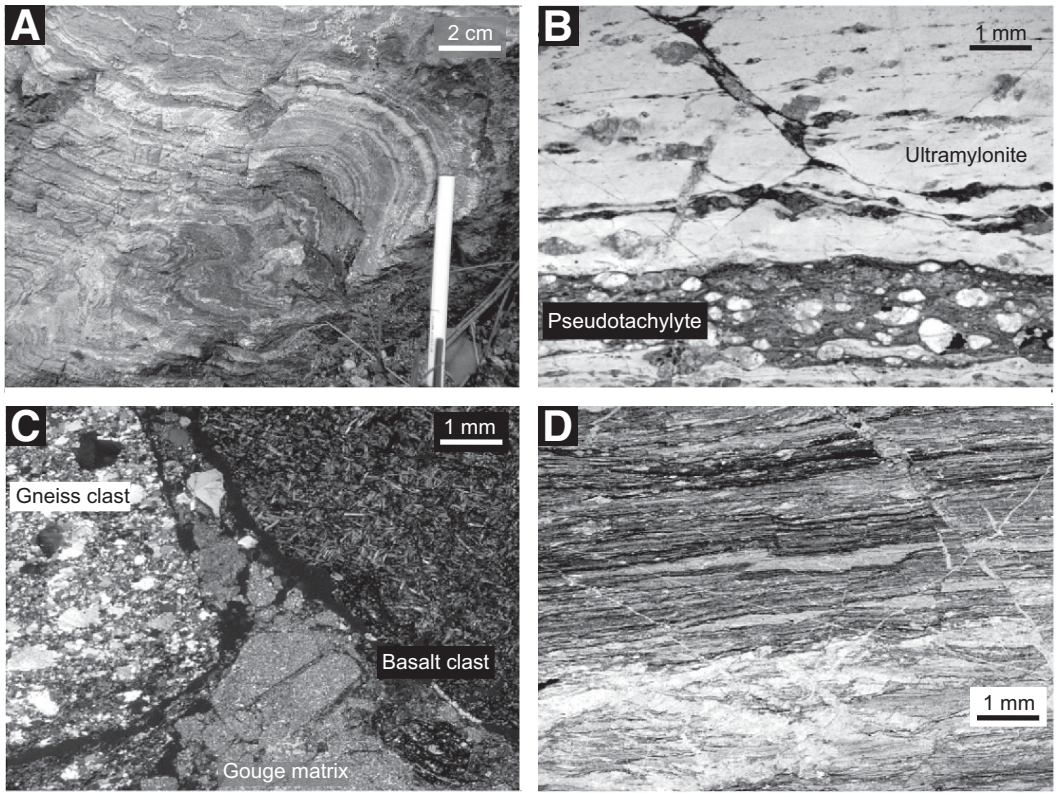

Figure 6. Evidence for ultramylonite, brittle overprinting and alteration within upper levels of Okanagan Valley shear zone. (A) Fold in silicified, chloritic ultramylonite; note ptygmatic folding of quartz-rich folia. (B) Photomicrograph of parallel porphyroblastic ultramylonite and pseudotachylyte layers. (C) Gouge-cemented cataclasite composed of equant clasts of upper-plate (basalt) and Okanagan Valley shear zone rocks (gneiss). (D) Ultramylonite overprinted by pervasive fracturing.

outliers such as these are found throughout the region as far east as the Grand Forks complex (Fig. 1), and are suggested to have been part of a single continuous sequence (Tempelman-Kluit and Parkinson, 1986; Parrish et al., 1988).

High-Angle Normal Faults

The Okanagan Valley shear zone, upper and lower plates, are crosscut and offset by a pervasive array of parallel, high-angle (~80°) normal faults trending NNE-SSW, perpendicular to the downdip elongation lineation in the Okanagan Valley shear zone. Normal faults trending NNE-SSW are characteristic of the southern Shuswap metamorphic complex (Fig. 1), for example, in the Republic graben and along the margins of the Grand Forks–Kettle River gneiss complex (Parrish et al., 1988; Laberge and Pattison, 2007).

Such faults form characteristic stair-stepping arrays with throw down to the WNW; the inferred extension direction is very similar to that recorded by linear fabric elements in the gneiss. Single, planar normal faults typically truncate and offset S_T and S_M; however, within the paragneiss, slip has been partitioned between shorter, en echelon fault pairs that utilize lithological boundaries as stepovers. An anomalously thick (≤15 cm) pseudotachylyte is developed along one of these stepovers, suggesting that the stepover surface served as an accommodation space during seismogenic slip. Sustained reactivation of gneissosity through the Eocene is discussed further in Eyal et al. (2006).

U-Pb GEOCHRONOLOGY

Analytical Methods

U-Pb dating of zircon was undertaken using both laser ablation–inductively coupled plasma–mass spectrometry (LA-ICP-MS) at Washington State University (analytical methods after Chang et al., 2006) and sensitive high-resolution ion microprobe (SHRIMP) at the Geological Survey of Canada (analytical methods after Stern, 1997; Stern and Amelin, 2003). Refer to Appendix B for a complete description of the geochronological techniques used and the treatment of the data, including common Pb corrections. Zircon standards and unknowns for both sets of analyses were mounted in 2.5-cm-diameter epoxy pucks that were ground and polished to expose the interiors of the grains. Cathodoluminescence (CL) and backscattered electron (BSE) images of the polished zircon were taken to characterize the internal features of the zircon and to provide a base map for targeting the spot analyses.

Data are presented as weighted average ages (e.g., Fig. 7); full analytical data tables are available in the data repositories (DR2 and DR3 [see footnote 1]). Tera-Wasserburg (TW) concordia plots were made using IsoPlot 3.0 (Ludwig, 2003). Ages are interpreted using weighted means of $^{206}Pb/^{238}U$ ages at the 95% confidence level (2σ error) unless otherwise noted. The ages of the single data points are also given with 2σ errors. Uncertainties on the ages when determined using weighted mean calculations tend to be unrealistically low and do not adequately account for the uncertainty in the U-Pb bias and cryptic matrix effects between standards and samples, which are difficult, if not impossible, to quantify. In order to account for these effects, a blanket 2% uncertainty should be considered when interpreting all of the U-Pb ages in this study.

A Comment on Polymodal Zircon Populations

The majority of samples in this study exhibit polymodal zircon populations. This is thought to result from a combination of: (1) multiple phases of zircon crystallization and rim growth, (2) metamorphic recrystallization of zircon, or (3) inheritance of xenocrystic zircon. Therefore, Th/U ratios, grain morphology, and CL zoning patterns are combined to characterize the subpopulations and give context to the different ages measured (e.g., Rubatto and Gebauer, 2000). Th/U ratio values ≥0.2 are considered typical of magmatic zircon. Metamorphic zircon is commonly anhedral (e.g., resorbed margins, rounded) with patchy or diffuse internal zonation under CL (Corfu et al., 2003), in contrast to euhedral magmatic zircon, which has well-defined internal zonation (e.g., oscillatory and sector; Crowley et al., 2008).

Plutonic Rocks of the Okanagan Valley Shear Zone and Footwall

Sample SB-24-6 (LA-ICP-MS)—K-Feldspar–Plagioclase–Quartz–Biotite Granodiorite

SB-24-6 is a sample of nonfoliated granodiorite from the Okanagan batholith in the footwall of the Okanagan Valley shear zone (Fig. 2). The zircons form one population of 50.7 ± 0.6 Ma (n = 21, mean square of weighted deviates [MSWD] = 1.5; GSA Data Repository DR2 [see footnote 1]), prismatic euhedral grains with oscillatory zoning (Figs. 7A and 7B). This is interpreted as igneous crystallization of a previously unrecognized Eocene pluton within the Okanagan batholith.

Sample SB-11-15b (LA-ICP-MS)—Plagioclase–K-Feldspar–Hornblende Diorite

Sample SB-11-15b is nonfoliated diorite of the informally named "Bighorn Sheep pluton" within the Okanagan batholith and Okanagan Valley shear zone footwall (Fig. 2), where diorite is crosscut by 53–51 Ma felsic sheets (Brown, 2010). Zircon crystals in the diorite are large, prismatic, euhedral and subhedral, oscillatory-zoned grains, occasionally with anhedral cores (Fig. 7C). There is one dominant zircon population (Fig. 7D) of 104 ± 1 Ma (n = 17, MSWD = 3.8), although there is a variation in age of older cores (ca. 140–ca. 208 Ma). The ca. 104 Ma age is interpreted as the crystallization age of the Bighorn Sheep pluton; older cores are interpreted to be xenocrysts incorporated from the country rock, including the protoliths to the amphibolite paragneiss domain.

Sample SB-07-12 (LA-ICP-MS)—K-Feldspar–Porphyritic Coryell Syenite

Sample SB-07-12 was collected from an exposure of variably foliated, K-feldspar–porphyritic Coryell syenite within the Okanagan Valley shear zone (Fig. 2). The zircons form one population of 50.2 ± 0.4 Ma (n = 26, MSWD = 0.82), consisting of subhedral and euhedral grains with oscillatory and sector zoning (Figs. 7E and 7F). This is interpreted as pre- or syntectonic, igneous crystallization within the Okanagan Valley shear zone, and it is consistent with other ages measured in the Coryell syenite (e.g., Parrish et al., 1988).

Plutonic Rocks—Summary

Identification of a uniquely Eocene juvenile magmatic component (50.7 ± 0.6 Ma) within the Okanagan batholith challenges the interpretation, hitherto poorly constrained, that the batholith was assembled in the Mesozoic, specifically Middle Jurassic through Cretaceous (e.g., Tempelman-Kluit, 1989). This age, and a review of Okanagan batholith ages in the literature (e.g., Breitsprecher and Mortensen, 2004) suggest that a significant part of the batholith crystallized in the Eocene, broadly contemporaneous with emplacement of the Coryell syenite (alkaline; Tempelman-Kluit, 1989) and Ladybird granite (S-type; Carr, 1992; Hinchey and Carr, 2006). The Okanagan batholith awaits a dedicated petrological and geochronological study.

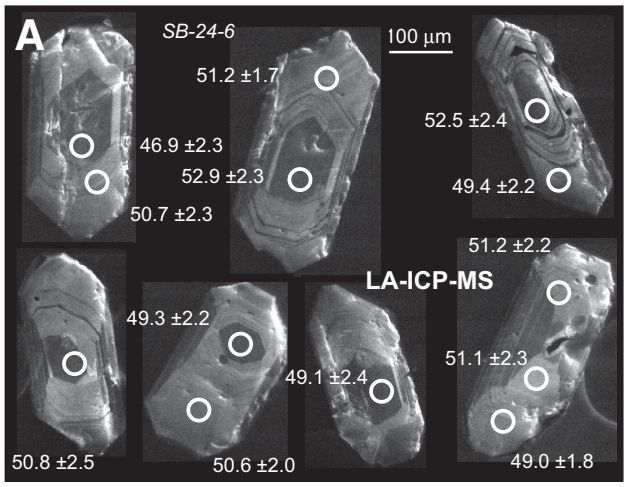

SB-24-6 - K-feldspar-plagioclase-quartz-biotite granodiorite

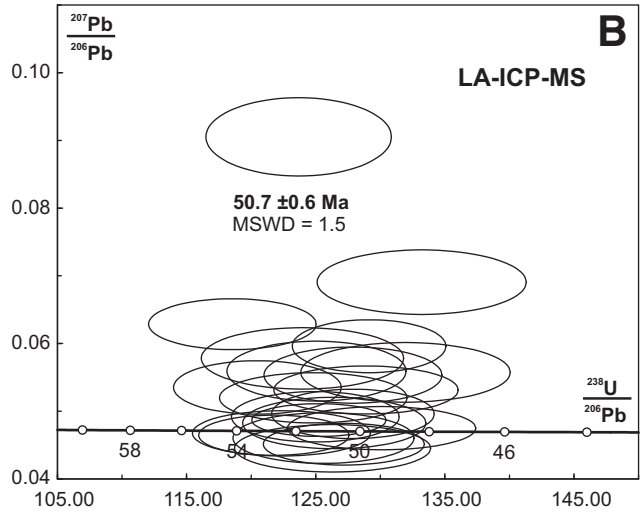

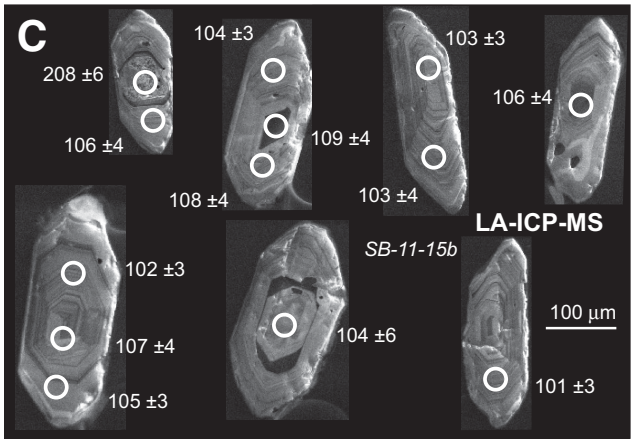

SB-11-15b - plagioclase-K-feldspar-hornblende diorite

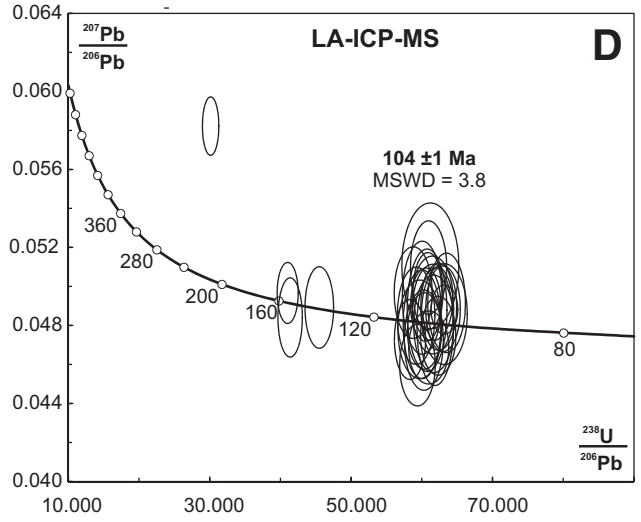

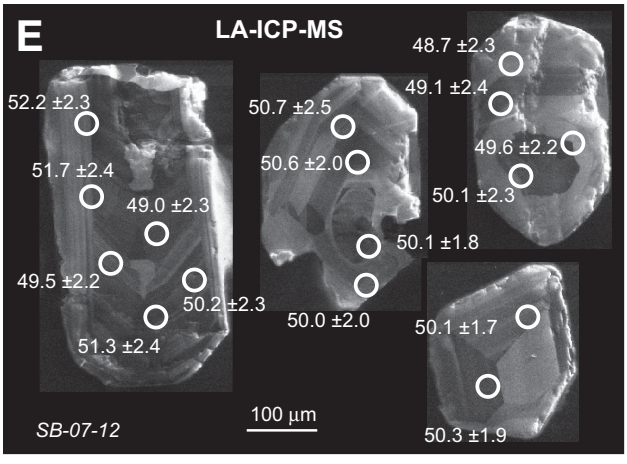

SB-07-12 - K-feldspar porphyritic Coryell syenite

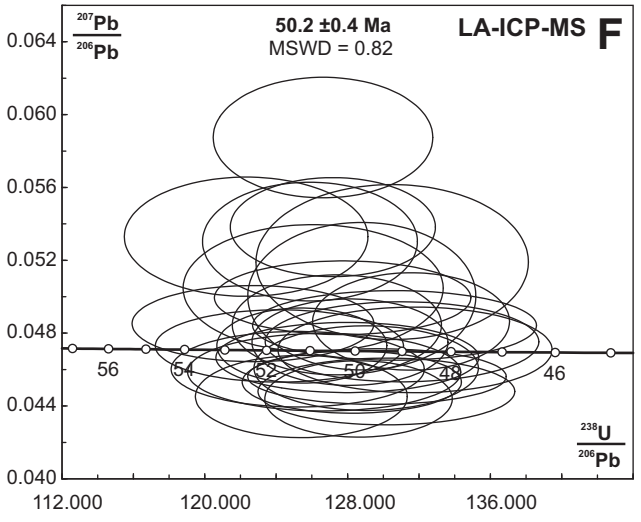

Figure 7. U-Pb geochronology of plutonic rocks within the Okanagan Valley shear zone and footwall. (A) Selection of cathodoluminescence (CL) zircon images showing analysis spot locations and $^{206}Pb/^{238}U$ spot age in Ma for sample SB-24-6. (B) Tera-Wasserburg (T-W) concordia for sample SB-24-6 with weighted mean ages of zircon in Ma (2σ error). (C–D) Paired CL zircon images and T-W concordia from sample SB-11-15b. (E–F) Paired CL zircon images and T-W concordia from sample SB-07-12. LA-ICP-MS—laser ablation–inductively coupled plasma–mass spectrometry; MSWD—mean square of weighted deviates.

Moreover, the only Mesozoic plutonic rocks here identified in the Okanagan Valley shear zone footwall are from the informally named Bighorn Sheep pluton, a 104 ± 1 Ma (Cretaceous) diorite. The Bighorn Sheep pluton is contemporaneous with the Cosens Bay pluton near Vernon (Fig. 1; 102.2 Ma; Glombick et al., 2006b), parts of the Oliver pluton (Sinclair et al., 1984), the Summit Creek stock (Irving et al., 1995), and the Spences Bridge magmatic arc (ca. 105–100 Ma; Irving and Thorkelson, 1990; Diakow and Barrios, 2009), and it is similar in age to the Okanogan Range batholith (ca. 114–107 Ma; Hurlow and Nelson, 1993).

The 50.2 ± 0.4 Ma Coryell syenite (this study) is syntectonic and coeval with the volcanic, alkaline Marron Formation (Souther, 1991) in the White Lake basin and hanging-wall klippen; they are likely comagmatic. Contemporaneous (1) deposition of the Marron Formation into hanging-wall graben, and (2) ductile deformation of the Coryell syenite within the Okanagan Valley shear zone indicate significant strain within (i.e., motion across) the Okanagan Valley shear zone at ca. 50 Ma.

Okanagan Gneiss—Paragneiss Domain

Sample SB-08-21 (SHRIMP)—K-Feldspar–Hornblende–Quartz Amphibolite Gneiss

SB-08-21 is from a <10-cm-thick layer of subhorizontal, foliated, and boudinaged, isoclinal-folded mesocratic amphibolite within the paragneiss domain, intercalated with centimeter-thick pegmatitic layers and meter-thick psammite (Fig. 8A). Zircon crystals are subhedral to anhedral with both oscillatory and sector-zoning (Fig. 9A), and Th/U values range from 0.01 to 0.50 (GSA Data Repository DR3 [see footnote 1]), suggesting both multiple processes of magmatic zircon crystallization and metamorphic recrystallization (e.g., Hoskin and Schaltegger, 2003; Rubatto and Gebauer, 2000).

There are two age peaks that we use as the preferred ages for this sample, 159 ± 2 Ma (n = 8, MSWD = 2.2) and 93.7 ± 3.6 Ma (n = 4, MSWD = 4.2) (Fig. 9B). Jurassic zircon crystals typically exhibit oscillatory zoning

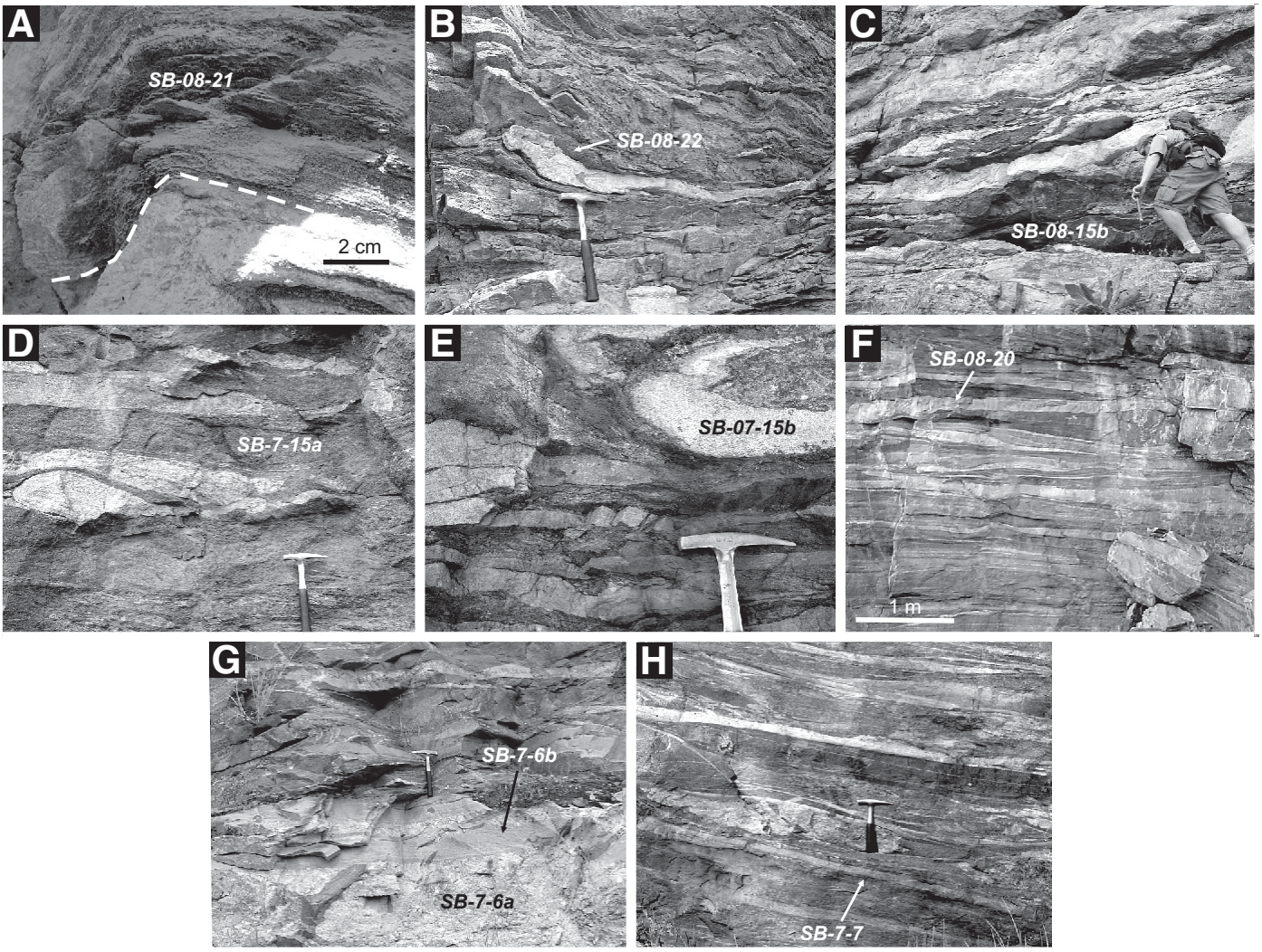

Figure 8. Field relationships of geochronology samples. (A) Paragneiss amphibolite sample SB-08-21. (B) Leucocratic paragneiss sample SB-08-22. (C) Ultramafic boudin sample SB-08-15b. (D) Migmatite sample SB-7-15a. (E) Leucosome sample SB-7-15b. (F) Leucosome layer SB-08-20. (G) Pegmatite sample SB-7-6a intruded by granite sheet sample SB-7-6b. (H) Granite sheet sample SB-7-7.

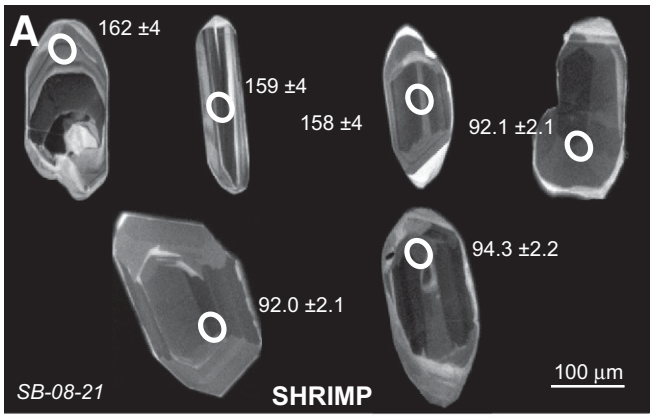

SB-08-21 - K-feldspar-hornblende-quartz amphibolite

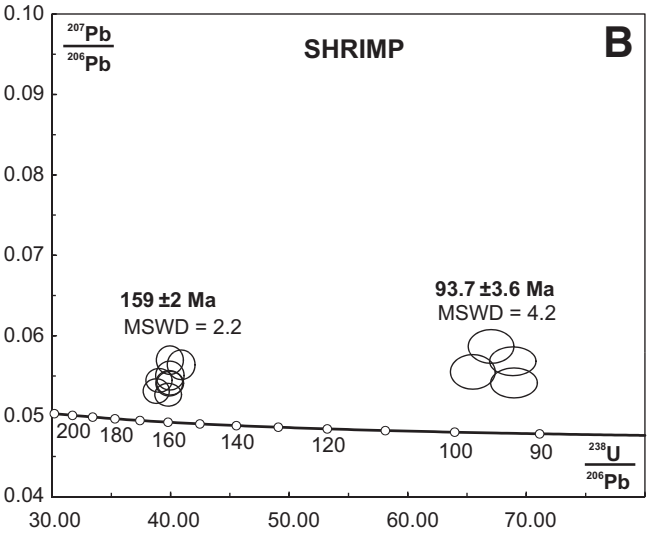

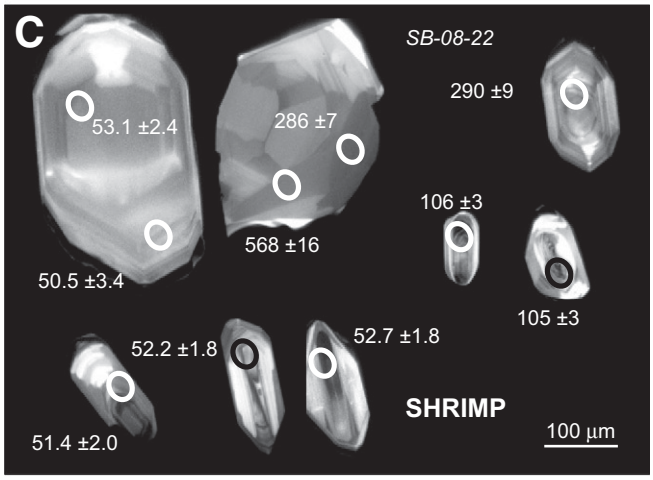

SB-08-22 - K-feldspar-quartz-hornblende layer

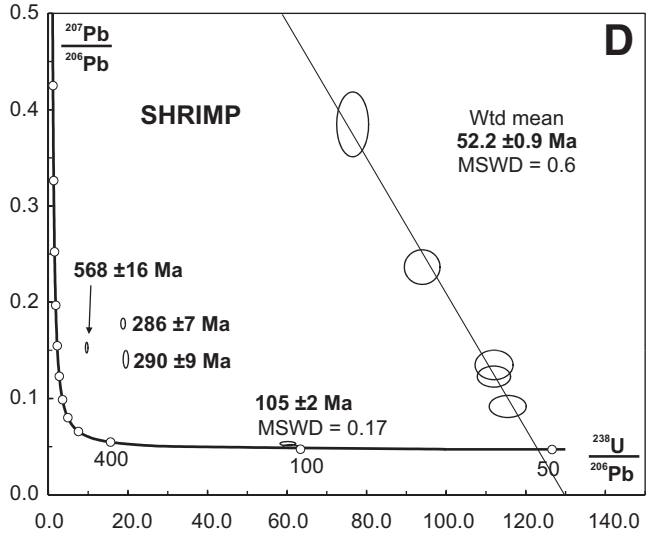

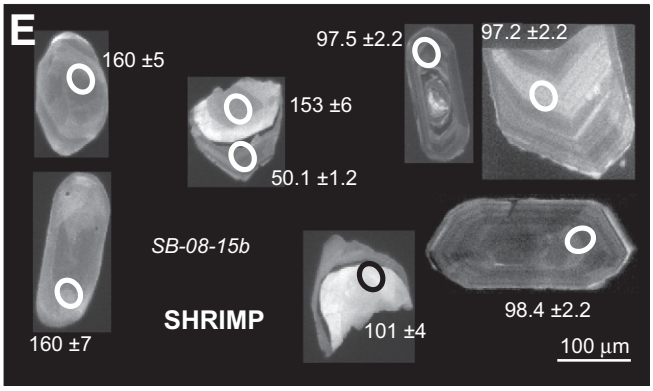

SB-08-15b - hornblende-clinozoisite amphibolite pod

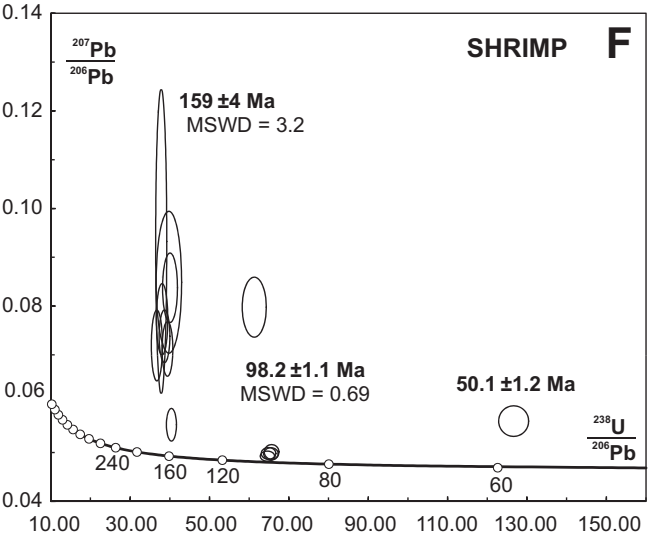

Figure 9. Paragneiss domain U-Pb geochronology. (A) Selection of cathodoluminescence (CL) zircon images showing analysis spot locations and $^{206}Pb/^{238}U$ spot age in Ma (^{207}Pb corrected; 2σ error) for sample SB-08-21. (B) Tera-Wasserburg (T-W) concordia for sample SB-08-21 with weighted mean ages of zircon in Ma (2σ error). (C–D) Paired CL zircon images and T-W concordia from sample SB-08-22 (common Pb line projected through Eocene subpopulation). (E–F) Paired CL zircon images and T-W concordia from sample SB-08-15b. SHRIMP—sensitive high-resolution ion microprobe; MSWD—mean square of weighted deviates.

(Fig. 9A) and have Th/U values up to 0.5. In contrast, Cretaceous zircon crystals are commonly diffusely sector zoned, and have low Th/U values (≤0.02). It is likely that these zircons come from small veinlets of Cretaceous leucosome, possibly related to partial melting of the host that were mixed in with the sample. The Jurassic age (159 ± 2 Ma) is interpreted to represent magmatic zircon crystallization; the Cretaceous age (93.7 ± 3.6 Ma) is interpreted to record an overprinting metamorphic event and/or intrusion of a minor amount of melt.

Sample SB-08-22 (SHRIMP)—K-Feldspar–Quartz–Hornblende Layer

SB-08-22 (Fig. 8B) is from an isoclinally folded, laterally discontinuous, foliated, coarse-grained, leucocratic K-feldspar–quartz–hornblende layer within the paragneiss domain, intercalated with amphibolite layers (e.g., SB-08-21). Field and petrographic evidence for the protolith of this layer is ambiguous; it is strongly sheared (e.g., rotated porphyroclasts) and is likely to be a metamorphosed felsic intrusion. Zircon crystals from this sample have diverse morphologies and sizes; crystals are euhedral to anhedral and have oscillatory and sector zoning (Fig. 9C). Th/U values (GSA Data Repository DR3 [see footnote 1]) are predominantly within the "magmatic" range (0.19–0.45).

Four ages are preserved in this sample (Fig. 8D): 568 ± 16 Ma (n = 1), ca. 288 Ma (n = 2), 105 ± 2 Ma (n = 2, MSWD = 0.17), and 52.2 ± 0.9 Ma (n = 5, MSWD = 0.6). The age for this sample is ambiguous. Both ca. 105 Ma and ca. 52 Ma zircons have zoning that would suggest magmatic origin (Fig. 9C). It is possible that the K-feldspar–quartz–hornblende layer intruded at ca. 105 Ma and then underwent partial melting or was injected with melt at ca. 52 Ma. The ca. 568 Ma and 288 Ma ages (Fig. 9D) are inferred to belong to zircon xenocrysts inherited from the country rock.

Sample SB-08-15b (SHRIMP)—Clinozoisite-Bearing Amphibolite Pod

SB-08-15b (Fig. 8C) is from a 1-m-thick melanocratic, coarse-grained, hornblende-clinozoisite-biotite ultramafic boudin, surrounded by psammitic, pegmatitic, and amphibolitic layers within the paragneiss domain. Zircon crystals (Fig. 9E) divide into three groups: (1) 159 ± 4 Ma (n = 8, MSWD = 3.2; Fig. 9F) anhedral, patchy, sector-zoned grains with transitional Th/U values (≤0.2); (2) 98.2 ± 1.1 Ma (n = 5, MSWD = 0.69) subhedral, oscillatory-zoned grains with low Th/U values (0.05–0.07); and (3) a single subhedral, 50.1 ± 1.2 Ma, low-Th/U (0.01), oscillatory-zoned rim around an anhedral, sector-zoned, 153 Ma core.

The Jurassic zircon crystals have ages very similar to the other mafic bodies dated in this study, contain faint oscillatory zoning (i.e., magmatic), and thus are interpreted to constrain the age of intrusion. The Cretaceous zircons display oscillatory zoning and are interpreted to have likely formed during ca. 98 Ma partial melting of the ca. 160 Ma host rock based on their uniformly low Th/U values. The ca. 50 Ma rim is interpreted to reflect an Eocene episode of metamorphism and partial melting leading to the crystallization of zircon rims onto older zircon grains.

Okanagan Gneiss—Migmatite Domain

Sample SB-07-15a (LA-ICP-MS)—Plagioclase-Hornblende-Quartz Melanosome

SB-07-15a (Fig. 8D) is a sample of foliated, folded, and mylonitized, coarse-grained, equigranular, plagioclase-hornblende-microcline-quartz melanosome from a 20-cm-thick layer within the migmatite domain. It preserves an elongation lineation trending 285°, and is surrounded by pegmatitic, granitic, and amphibolitic layers, and parallel to thin leucosome veins. Samples 07-15a, 07-15b, 08-20, and 7-6b were collected from the same location (Fig. 2). The zircon crystals (Fig. 10A) are ubiquitously 162 ± 1 Ma (n = 38, MSWD = 1.3; Fig. 10B).

We interpret 162 ± 1 Ma to be an igneous crystallization age because of their euhedral grain morphologies, and the presence of both oscillatory and sector zonation. Some grains show higher luminescence patchy zoning around the rims, but these were too narrow to analyze. Overprinting rims are presumably the result of later partial recrystallization during metamorphism or the addition of small amounts of new zircon growth during anatexis. The interpretation of this sample as residuum of the neosome (i.e., not a leucosome following anatexis) is consistent with the melanosome sharing a ca. 160 Ma protolith with the paragneiss domain.

Sample SB-07-15b (LA-ICP-MS)—Quartz–K-Feldspar–Plagioclase–Muscovite Leucosome

SB-07-15b is from a ≤8-cm-thick, isoclinally and recumbently folded leucosome sheet within the migmatite domain (Fig. 8E). It is folded together with amphibolite layers, transposed, mylonitized, and preserves an elongation lineation trending 285°. The zircon population is dominated by euhedral and subhedral, equant, oscillatory-zoned, ca. 53 Ma grains but also includes rare anhedral pre-Cenozoic cores with ca. 53 Ma rims (Fig. 10C). The weighted mean age of Eocene zircons (rims and whole grains) is 52.9 ± 0.9 Ma (n = 17, MSWD = 2.9; Fig. 10D); the elevated MSWD indicates some slight mixing of ages, but the greatest numbers of concordant ages are clustered around 52.9 ± 0.9 Ma. We interpret this to be the age of anatectic melting to form the migmatite domain. Older cores with $^{207}Pb/^{206}Pb$ ages of 1712 ± 28 Ma and 615 ± 38 Ma (Fig. 10D) are inferred to be xenocrysts inherited from the country rock.

Sample SB-08-20 (SHRIMP)—Quartz–K-Feldspar Leucosome

SB-08-20 is from a ≤10 cm-thick, transposed, subhorizontal, mylonitized leucosome layer in the migmatite domain (Fig. 8F). Multiple ages are recorded from the recovered zircons (Fig. 11A). Five anhedral, faintly zoned grains with magmatic (≥0.27) Th/U values yield a weighted mean Pb/U age of 200 ± 2 Ma (MSWD = 1.0; Fig. 11B) (GSA Data Repository DR3 [see footnote 1]), while three anhedral, faintly zoned zircons with variable Th/U values (0.03–0.46) give a slightly younger weighted mean age of 189 ± 8 Ma (n = 3, MSWD = 1.7). Both of these subpopulations are interpreted as xenocrysts derived from the country rock, perhaps the coeval and adjacent Nicola magmatic arc (Woodsworth et al., 1991; Tempelman-Kluit, 1989). Two U-rich, anhedral, faintly zoned zircons yield ages of 170–180 Ma and low Th/U values (≤0.01). These analyses suggest that there is likely a Jurassic population similar in age to that found in the melanosome (SB-07-15A). Other U-rich zircons are subhedral, porous, and partly oscillatory zoned and have low Th/U values (0.03). They range in age from 58 to 63 Ma, with the youngest grain recording the lowest concentration of U (3719 ppm). Because the matrix effect leads to a greater deviation in age with increasing U content, 58 Ma can only be considered the maximum age of this subpopulation of grains. Finally, a single subhedral, faintly zoned zircon with low U (182 ppm) and a Th/U value of 0.44 yields an age of 52.9 ± 1.4 Ma, which is interpreted to be the product of crystallization from an anatectic melt.

Sample SB-7-6a (LA-ICP-MS)—Quartz–K-Feldspar–Plagioclase–Almandine–Biotite Pegmatite

SB-7-6a is from a ≥1-m-thick, massive (i.e., nonfoliated) pegmatite layer within the migmatite domain, where it is crosscut by a thin granite sheet (SB-7-6b; Fig. 8G). It contains rafts of foliated amphibolite gneiss, and it likely was intruded into the surrounding subhorizontally layered amphibolite gneiss.

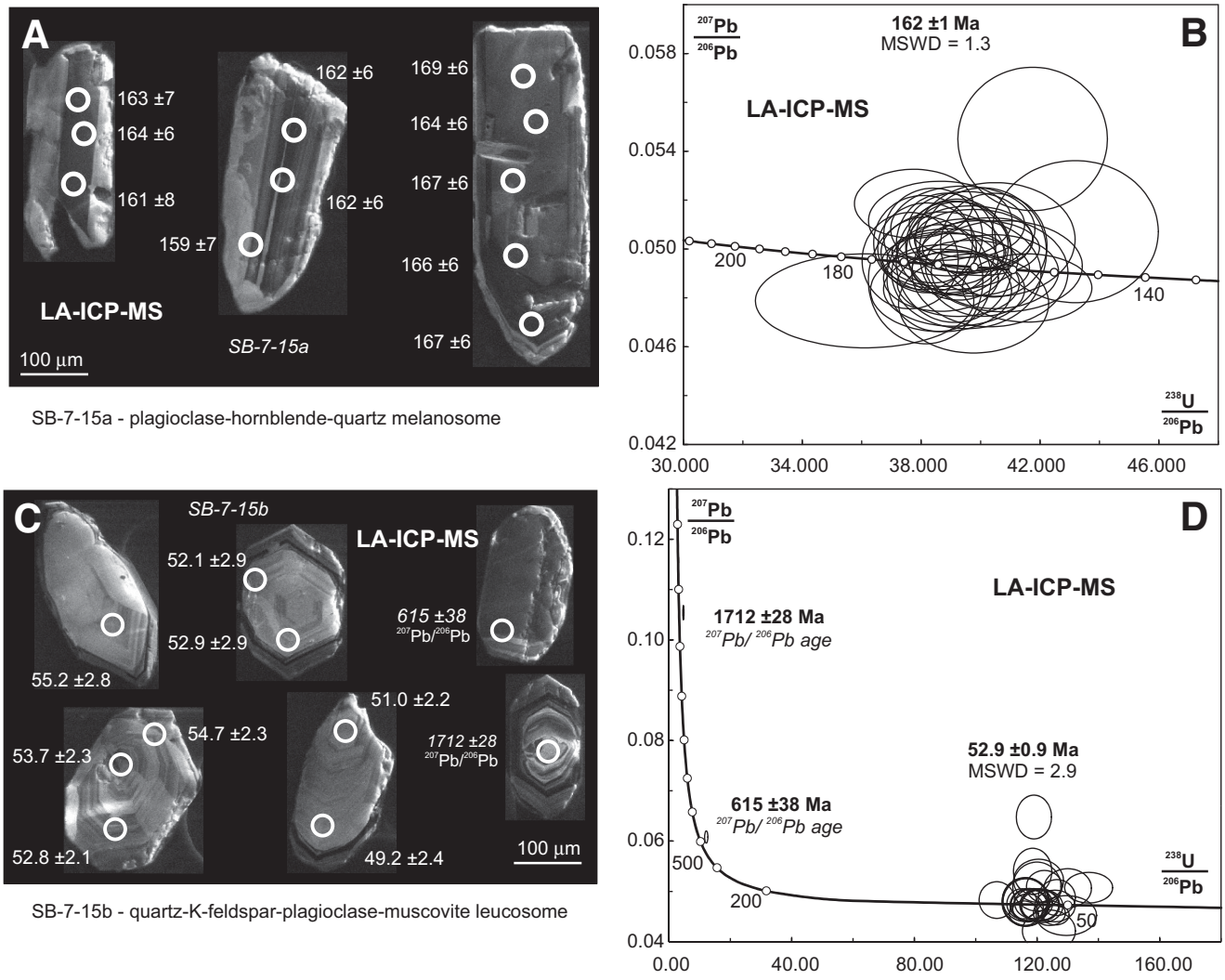

Figure 10. Migmatite domain U-Pb geochronology. (A) Selection of cathodoluminescence (CL) zircon images showing analysis spot locations and $^{206}Pb/^{238}U$ spot age in Ma (^{207}Pb corrected; 2σ error) for sample SB-7-15a. (B) Tera-Wasserburg (T-W) concordia for sample SB-7-15a with weighted mean ages of zircon in Ma (2σ error). (C–D) Paired CL zircon images and T-W concordia from sample SB-7-15b. LA-ICP-MS—laser ablation–inductively coupled plasma–mass spectrometry; MSWD—mean square of weighted deviates.

Zircons form three subpopulations (Fig. 11C): (1) euhedral and subhedral, sector- and oscillatory-zoned, 91.7 ± 1.8 Ma (intercept age; n = 16, range ca. 97–87 Ma, MSWD = 6.3; Fig. 11D) grains; (2) subhedral, ca. 92 Ma cores surrounded by ca. 83 Ma rims (n = 3); and (3) anhedral, sector-zoned, 50.7 ± 1.4 Ma grains (n = 2). The interpreted zircon crystallization age is ca. 92 Ma; a precise age cannot be given due to the scatter (Fig. 11D). Circa 83 Ma rims and ca. 50.7 Ma grains probably represent metamorphic crystallization and recrystallization, respectively, or new growth of rims during anatexis.

Okanagan Gneiss—Summary

None of the Okanagan gneiss layers sampled has zircon age populations that indicate a significant Proterozoic protolith as inferred by Armstrong et al. (1991). The ages of zircon from the heterolithic paragneiss and migmatite domains are correspondingly heterogeneous. Paragneiss and migmatite domains yield abundant magmatic ca. 160 Ma (Jurassic) zircon, often with Cretaceous (ca. 90 Ma) and/or Eocene (ca. 53–50 Ma) rims; magmatic-looking crystals are likely related to partial melting of the host rock at that time. A Jurassic zircon population is prevalent throughout the more mafic component of the Okanagan gneiss, and it is inferred to be the age of mafic or intermediate magmas intruding a sedimentary protolith. Important younger age populations of ca. 90 Ma and ca. 53–50 Ma record phases of high-temperature metamorphism in the Okanagan gneiss, further magmatism, or crustal anatexis; similar bimodal populations have been identified in the Tonasket gneiss (Okanogan Dome; Kruckenberg et al., 2008).

Felsic Sheets

Both the Okanagan gneiss and the footwall are crosscut by a multitude of peraluminous, granite and granitic pegmatite sheets, many of which postdate some or all folding and transposition within the gneiss; they are variably discordant to S_T and may or may not be folded. All the felsic

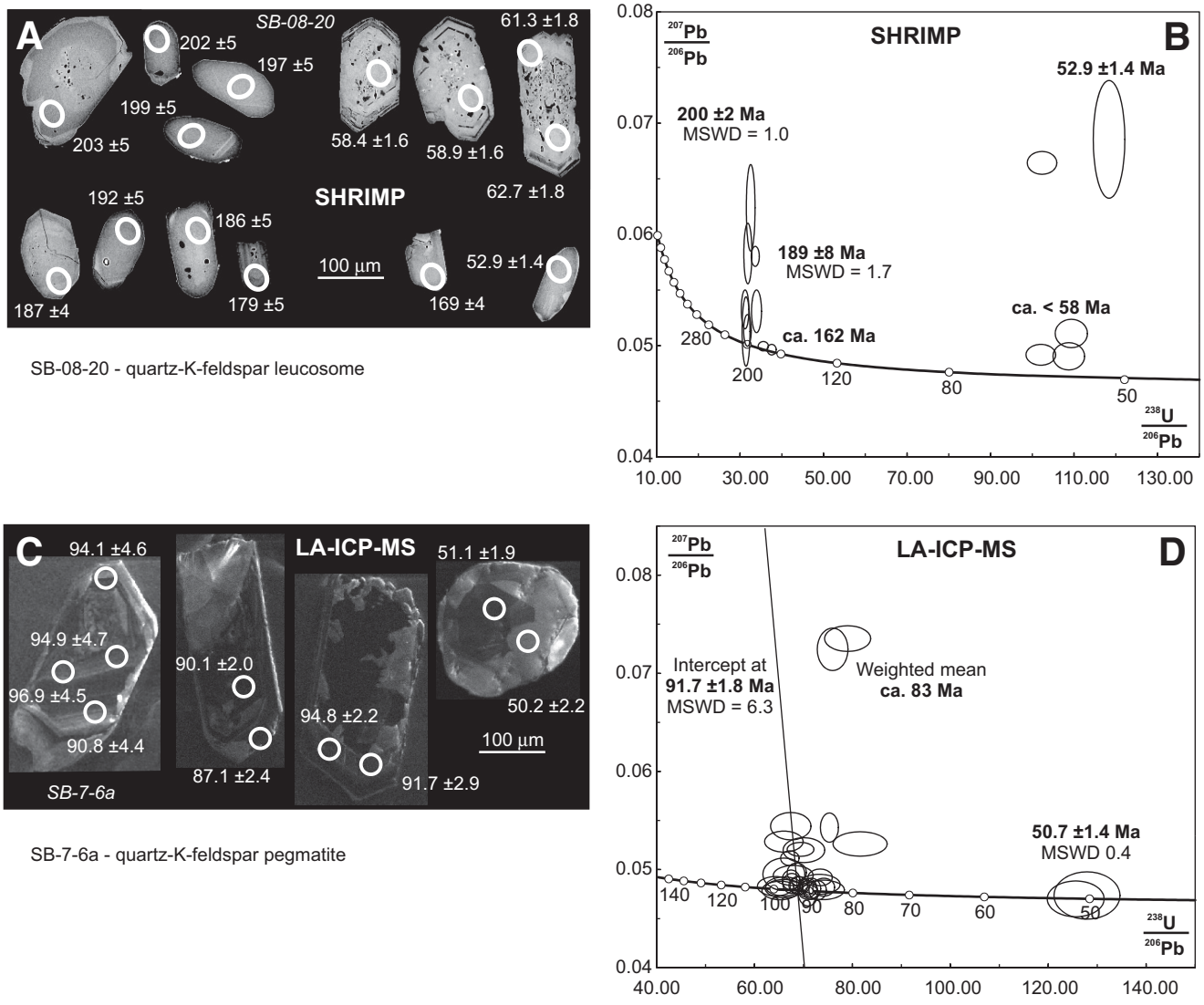

SB-08-20 - quartz-K-feldspar leucosome

SB-7-6a - quartz-K-feldspar pegmatite

Figure 11. Migmatite domain U-Pb geochronology. (A) Selection of cathodoluminescence (CL) zircon images showing analysis spot locations and $^{206}Pb/^{238}U$ spot age in Ma (^{207}Pb corrected; 2σ error) for sample SB-08–20. (B) Tera-Wasserburg (T-W) concordia for sample SB-08–20 with weighted mean ages of zircon in Ma (2σ error). (C–D) Paired CL zircon images and T-W concordia from sample SB-7–6a. SHRIMP—sensitive high-resolution ion microprobe; LA-ICP-MS—laser ablation–inductively coupled plasma–mass spectrometry; MSWD—mean square of weighted deviates.

sheets exhibit a weak to moderate planar fabric (S_M) that likely developed during the latest stages of solid-state deformation imposed by the Okanagan Valley shear zone.

Sample SB-7-7 (SHRIMP and LA-ICP-MS)—K-Feldspar–Quartz–Hornblende Granite

Sample SB-7-7 is from a 5–8-cm-thick granite sheet in the migmatite domain. It is slightly oblique to the transposed, <10° west-dipping lithological layering within the migmatite domain, where it truncates S_T, recumbent, isoclinal folds, and leucosome stromata (Fig. 8H). The sheet is weakly boudinaged and is overprinted by a subhorizontal protomylonitic fabric (S_M). Based on overprinting field relationships alone, this is the youngest felsic intrusion we know of in the Okanagan gneiss.

Zircons form two subpopulations: euhedral and subhedral, sector- and oscillatory-zoned (Fig. 12A), 51.6 ± 0.7 Ma (n = 10, MSWD = 1.8) grains (Fig. 12B) with magmatic Th/U values (0.22–0.60; GSA Data Repository DR2 [see footnote 1]); and two euhedral, prismatic, oscillatory-zoned, zircons that record ca. 92 Ma rims around anhedral cores dated at ca. 193 and ca. 106 Ma. Both cores and rims have transitional Th/U values (≤0.21). The interpreted crystallization age is 51.6 ± 0.7 Ma; a duplicate sample dated by LA-ICP-MS produced a mean weighted age of 51.0 ± 2.1 (n = 2, MSWD = 0.83). The ca. 92 Ma zircons were possibly entrained from similarly aged pegmatite (see previous section) crosscut by SB-7-7.

Sample SB-7-6b (LA-ICP-MS)—K-Feldspar–Quartz–Hornblende–Garnet Granite

SB-7-6b is from a 10–20-cm-thick foliated granite sheet within the migmatite domain. The sheet crosscuts a thick pegmatite sheet (SB-7-6a) and the amphibolitic migmatite, S_T, folds, and leucosome stromata (Fig. 8G); it is not folded. It is overprinted by a subparallel planar fabric

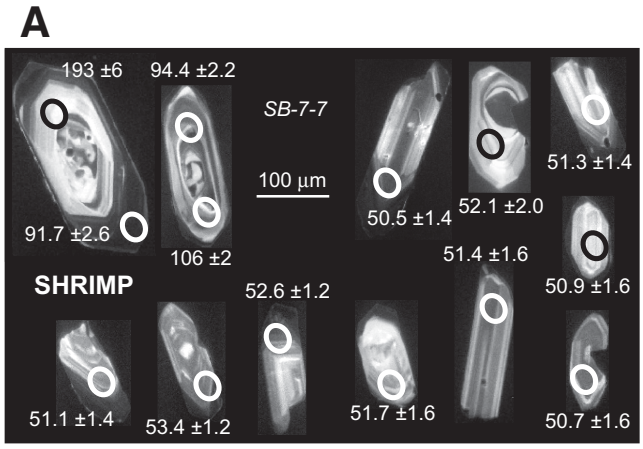

SB-7-7 - K-feldspar-quartz-hornblende granite

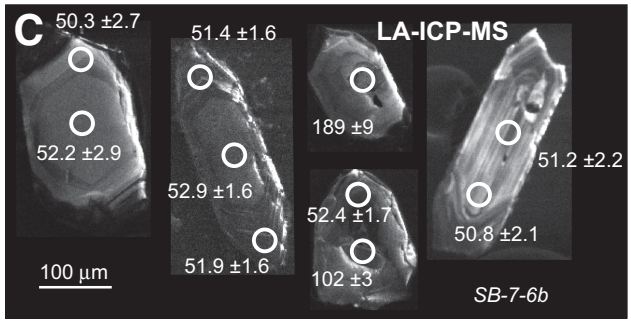

SB-7-6b - K-feldspar-quartz-hornblende-garnet granite

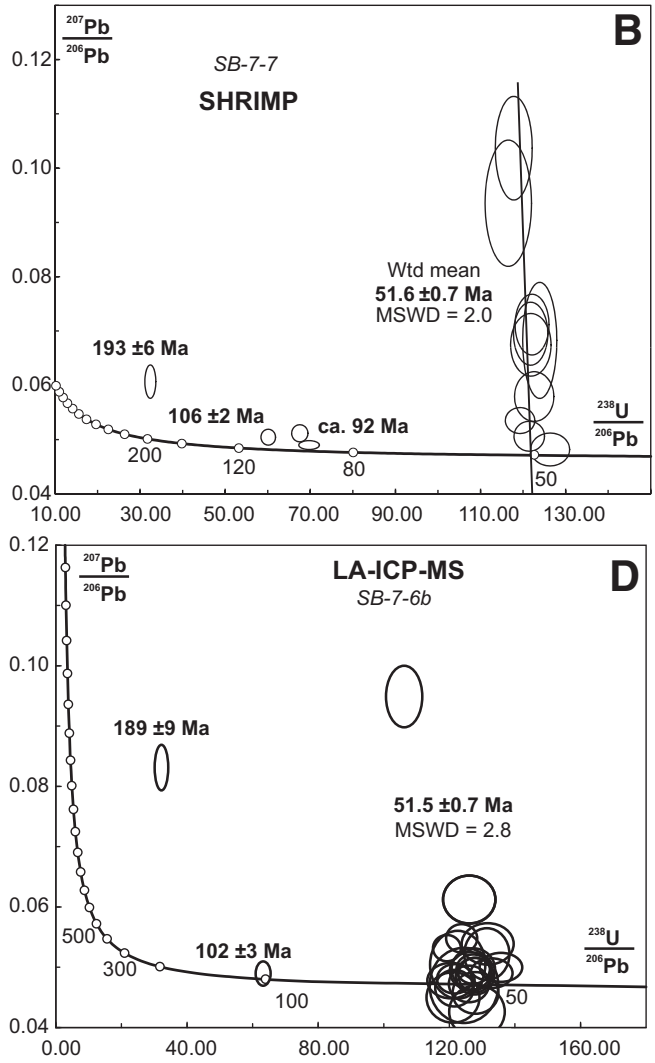

Figure 12. (A–B) Geochronology of crosscutting felsic intrusions, and field relations of granite sheet (SB-7-7) that intrudes the migmatite domain. (A) Selection of cathodoluminescence (CL) zircon images showing analysis spot locations and $^{206}Pb/^{238}U$ spot age in Ma (^{207}Pb corrected; 2σ error) for sample SB-7-7. (B) Tera-Wasserburg (T-W) concordia for sample SB-7-7 with weighted mean ages of zircon in Ma (2σ error). (C–D) Field relations of granite sheet (SB-7-6b) that intrudes the migmatite domain and pegmatite sheet SB-7-6a. Paired CL zircon images and T-W concordia from sample SB-7-6b (common Pb line projected through Eocene subpopulation). LA-ICP-MS—laser ablation–inductively coupled plasma–mass spectrometry; SHRIMP—sensitive high-resolution ion microprobe; MSWD—mean square of weighted deviates.

(S_M). Zircons form one population of euhedral and anhedral, sector- and oscillatory-zoned grains (Fig. 12C), with a mean age of 51.5 ± 0.7 Ma (n = 26, MSWD = 2.8; Fig. 12D); some grains have anhedral Mesozoic cores. We interpret 51.5 ± 0.7 Ma to be the igneous crystallization age and older cores as xenocrysts.

Felsic Sheets—Summary

Peraluminous felsic sheets were intruded at ca. 52 Ma, immediately postdating anatexis and leucosome injection at ca. 53 Ma as recorded by sample SB-7-15b. The felsic sheets appear to record the time of late-stage development of a shear zone foliation (S_M) and noncoaxial ductile deformation in the Okanagan Valley shear zone to at least ca. 51 Ma. These results are consistent with ages of other sheets intruded elsewhere in the Okanagan Valley shear zone that are strongly to weakly foliated, lineated, and mylonitized, including: ca. 51–50 Ma (Parrish et al., 1988), 51.7 ± 1.1 Ma and 53.5 ± 6.3 Ma (Brown, 2010), and 56 ± 1 Ma (Johnson, 1994). Furthermore, the pre- or syntectonic Coryell syenite (SB-07-12) has a crystallization age of 50.2 Ma (Fig. 7F); therefore, ductile deformation must have continued beyond 50.2 Ma, and the end is not constrained in this region. In the correlative Tonasket paragneiss-orthogneiss unit within the Okanogan Dome (Kruckenberg et al., 2008), the end of ductile deformation is constrained to ca. 49 Ma.

DISCUSSION

Origin, Age, and Evolution of the Okanagan Gneiss

Implications for Previous Age Estimates for the Okanagan Gneiss

Previous age estimates for the Okanagan gneiss, and the paragneissic domain specifically, have been late Paleozoic to early Mesozoic (e.g.,

Christie, 1973; Ryan, 1973; Parkinson, 1985) and Paleoproterozoic (Armstrong et al., 1991). Phanerozoic estimates were based largely on lithological similarities to metasedimentary rocks in the surrounding region and only very limited dating of xenocrystic cores.

Armstrong et al. (1991) analyzed samples from micaceous layers within the paragneiss using a combination of U-Pb zircon multigrain analysis, and Rb-Sr and Sm-Nd whole-rock analyses. They inferred a Paleoproterozoic protolith or protolith source based on (1) a Sm-Nd crustal residence age of 2230 ± 110 Ma, (2) a zircon source of 1899 ± 24.5 Ma (U-Pb upper intercept), and (3) a Rb-Sr isochron of 2059 ± 586 Ma. Their data can be interpreted one of two ways: either (1) the Okanagan paragneiss or its protolith were formed in the Paleoproterozoic, or (2) a protolith (of unconstrained age) was derived from a Paleoproterozoic igneous or metamorphic source. Armstrong et al. (1991) favored the former hypothesis because of the similarity in ages across all three of the radiometric systems utilized, and the understanding that protracted erosion, transport, and deposition would be unlikely to preserve similar patterns across multiple radiometric systems.

The Armstrong et al. (1991) interpretation that the Okanagan gneiss is a Paleoproterozoic unit (ca. 2.2–2.0 Ga) is important because it implies that the Okanagan gneiss is an exposed section of North American cratonic basement, analogous to those in the Monashee complex (Fig. 1; e.g., Wanless and Reesor, 1975). If this interpretation is correct, the Okanagan gneiss would be the westernmost unambiguous exposure of cratonic basement in the southern Canadian Cordillera (e.g., Armstrong et al., 1991; Parkinson, 1991; Crowley, 1999). This interpretation has been incorporated by numerous regional- and Cordilleran-scale geological maps (e.g., Wheeler and McFeely, 1991; Massey et al., 2005; Cui and Erdmer, 2009) and used in the interpretation of crustal-scale geophysical surveys (e.g., Cook et al., 1992; Cook, 1995).

New Data Suggest a Phanerozoic Protolith for the Okanagan Gneiss

In this paper, we infer a Phanerozoic age, probably Mesozoic, for the paragneiss protolith (Fig. 13). Inherited xenocrystic zircon cores as young as 188 Ma (Early Jurassic) are commonly found in the mafic amphibolite gneiss, the Okanagan batholith, and in the migmatite. In contrast to the Monashee gneiss domes (e.g., Armstrong et al., 1991; Crowley, 1997; Vanderhaeghe et al., 1999), no Paleoproterozoic or Archean zircons or zircon cores were identified. The mafic sheets that intruded and are now interleaved within the Okanagan gneiss are Middle Jurassic in age (ca. 160 Ma), not Paleoproterozoic, as is the case in the basement rocks of the Monashee complex (Parrish, 1995; Crowley, 1999). More tentatively, this interpretation is supported by the marine depositional setting of the paragneiss protolith (e.g., pelite, sandstone, marble), which is similar to that interpreted for the adjacent greenschist-facies sedimentary and volcaniclastic successions that comprise the late Paleozoic Kobau (Okulitch, 1973), Anarchist, and Harper Ranch Groups.

A Revised Tectonic Model

Our preferred model for deposition of the sedimentary protolith of the paragneiss domain requires deposition of terrigenous sediment into a late Paleozoic to Mesozoic marine basin between the western paleomargin of the Laurentian craton and the accreted Intermontane terranes. Sediment containing zircons with Precambrian and early Paleozoic cores suggests it was supplied, at least in part, from Precambrian North American cratonic basement or recycled basement. Exactly which part of the craton remains unclear and requires further investigation.

The sedimentary package was buried and metamorphosed between 180 and 160 Ma (e.g., Parrish, 1995; Fig. 13) before arc-backarc magmatism was re-established ca. 160 Ma (Brown, 2010; this study), and the metasedimentary protolith was pervasively intruded by mafic sheets. Metamorphism may have led to some anatexis at this time (e.g., Glombick, 2006b); although our data suggest that the ca. 160 Ma zircon population is magmatic rather than metamorphic, we do not discount the likelihood of Middle Jurassic contractional deformation, burial, and metamorphism in the region, as it was widespread throughout the southern Canadian Cordillera at this time (e.g., Monger et al., 1982; Parrish, 1995; Gibson et al., 2008). The metasedimentary package and mafic intrusions were subsequently intruded by the Okanagan batholith during protracted continental arc magmatism through the Late Jurassic and Early Cretaceous until ca. 105 Ma (Fig. 13).

The proto–Okanagan gneiss continued to be buried and metamorphosed to sillimanite-grade and amphibolite-facies in response to accretion of the Insular terranes at ca. 100–83 Ma (Monger et al., 1982; Gibson et al., 2008). These remained buried at midcrustal levels (~20 km; Fig. 4A) until exhumation along the Okanagan Valley shear zone in the Eocene (56–48 Ma; Fig. 12). There is an absence of any demonstrably pre-Eocene fabrics in the Okanagan gneiss; while Mesozoic metamorphism of the paragneiss domain protolith is likely, only in the Eocene did migmatization and deformation of both the paragneiss and felsic orthogneiss domains occur contemporaneously. Therefore, the Okanagan gneiss, as defined in this paper, is a lithotectonic unit that was established in the Eocene during deformation associated with the Okanagan Valley shear zone that transposed several different lithologic units within this marginal zone. The identification of a small-volume migmatite domain indicates that anatexis played a role during gneiss formation and deformation. Numerous models of crustal flow (e.g., Tirel et al., 2004; Rey et al., 2011) emphasize the involvement of melt-rich crust in rapid advection of deep crustal material toward the surface during lithospheric extension, often in concert with localized extensional shearing (brittle and ductile) in the upper crust (e.g., a detachment fault). Anatexis and melt-present ductile flow are demonstrated to have been important in the formation of the Okanogan Dome to the south (Kruckenberg et al., 2008; Kruckenberg and Whitney, 2011). We have not attempted to constrain the importance of melt-present ductile flow within the Okanagan gneiss due to the small volumes of migmatite identified; however, this warrants further investigation.

Regional Significance of the Okanagan Valley Shear Zone

The Okanagan Valley shear zone is widely interpreted to be a significant and important structure in the southern Canadian Cordillera. After the pioneering study of Tempelman-Kluit and Parkinson (1986) described the Okanagan Valley shear zone as a detachment bounding the Shuswap metamorphic complex within the Okanagan valley, subsequent studies have traced it, or its equivalents, to the north and south (Fig. 1). The significance of the Okanagan Valley shear zone as a major tectonic structure is apparent in several geological, geophysical, and geochemical studies. (1) The Okanagan Valley shear zone is assigned as the geological and geomorphological boundary between the rifted western margin of the ancestral North American craton and the Intermontane (accreted oceanic and arc terranes) belts in the southern Canadian Cordillera (e.g., Wheeler and McFeely, 1991). (2) The Okanagan Valley shear zone is inferred to be the surface expression of a prominent, shallowly west-dipping, upper- and midcrustal seismic reflector that separates allochthonous metasedimentary and metavolcanic rocks of the Intermontane terranes from parautochthonous gneisses of the Omineca belt (Cook et al., 1992). (3) The Okanagan Valley shear zone is broadly parallel and proximal to the positions of the ε_{Nd} (<0) and $^{87}Sr/^{86}Sr$ (>0.704) isopleths during the Jurassic, Cretaceous, and Paleogene (Armstrong, 1988; Ghosh, 1995b), which are inferred to

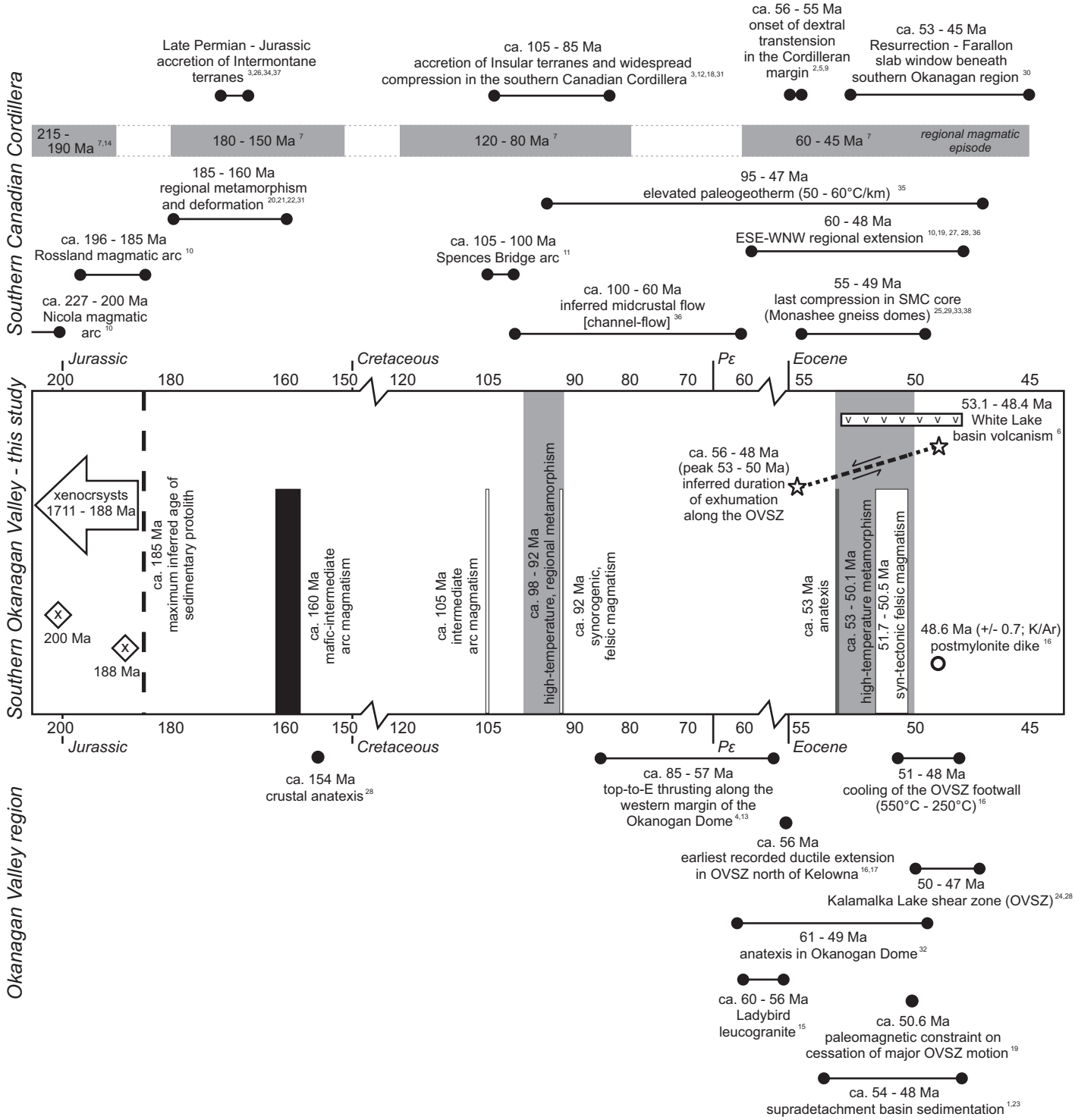

Figure 13. Time-event diagram (200–40 Ma) of orogenic, igneous, and metamorphic events in the southern Canadian Cordillera (top), this study (middle; box in middle), and elsewhere in the southern Okanagan Valley shear zone (OVSZ, bottom). Citations used: 1—Pearson and Obradovich (1977); 2—Ewing (1980); 3—Monger et al. (1982); 4—Goodge and Hansen (1983); 5—Engebretson et al. (1984); 6—Church (1985); 7—Armstrong (1988); 8—Lonsdale (1988); 9—Parrish et al. (1988); 10—Monger et al. (1991); 11—Irving and Thorkelson (1990); 12—McGroder (1991); 13—Potter and Zartman (1991); 14—Woodsworth et al. (1991); 15—Carr (1992); 16—Bardoux (1993); 17—Johnson (1994); 18—Monger and Journeay (1994); 19—Wingate and Irving (1994); 20—Murphy et al. (1995); 21—Parrish (1995); 22—Colpron et al. (1996); 23—Suydam and Gaylord (1997); 24—Heaman et al. (1999); 25—Crowley et al. (2001); 26—Monger and Price (2002); 27—Brown and Gibson (2006); 28—Glombick et al. (2006b); 29—Hinchey et al. (2006); 30—Madsen and Thorkelson (2006); 31—Gibson et al. (2008); 32—Kruckenberg et al. (2008); 33—Gervais et al. (2010); 34—Beranek and Mortensen (2011); 35—Crider and Callahan (2011); 36—Gervais and Brown (2011); 37—Nelson and Colpron (2011); 38—Spalla et al. (2011). SMC—Shuswap metamorphic complex; Pε—Paleocene.

demarcate the westernmost edge of cratonic basement that contaminated Mesozoic–Paleocene arc magmatism.

Finally, (4) the architecture and evolution of the Okanagan Valley shear zone can be used to constrain different models of crustal extension in the southern Canadian Cordillera, for example, midcrustal flow, gneiss dome development, etc. Specifically, the nascent Okanagan Valley shear zone could be inferred to correspond to the upper margin (normal-sense, top-down-to-the-west) of a ductile midcrustal channel inferred to have been active in the Cretaceous to Paleocene (Fig. 13; e.g., Brown and Gibson, 2006; Glombick et al., 2006b; Gervais and Brown, 2011). If this is indeed the case, then the Okanagan Valley shear zone would have a long history (Cretaceous to Eocene) and an important role in localizing midcrustal flow within the Shuswap metamorphic complex. Furthermore, extension across the Okanagan Valley shear zone may have been contemporaneous with compression elsewhere, for example, within the core of the Shuswap metamorphic complex (Gibson et al., 1999, 2008; Crowley et al., 2001). We do not find evidence of pre-Eocene ductile deformation, neither compressional nor extensional; therefore our data cannot be used to assess fully models of pre-Eocene midcrustal flow within the Shuswap metamorphic complex. However, our data demonstrate extension and ductile deformation in the southern Okanagan Valley shear zone between 56 and 50 Ma that are otherwise absent in parts of the upper margin of the proposed midcrustal channel farther north (Gervais and Brown, 2011). Further study is necessary to establish or refute any links between the purported Cretaceous–Paleocene midcrustal channel and the Eocene Okanagan Valley shear zone.

Given the significance of the Okanagan Valley shear zone, an understanding of the magnitude of extension across the Okanagan Valley shear zone is important. Several studies along the length of the Okanagan Valley shear zone have estimated the magnitude of extension; estimates typically increase from north to south, from ~30 km across the Okanagan–Eagle River section (Fig. 1; Johnson, 1994; Johnson and Brown, 1996), to 45–75 km at Kelowna (Bardoux, 1993), to ≤90 km across the Okanagan valley in the study area (Parkinson, 1985; Tempelman-Kluit and Parkinson, 1986). The study of Glombick et al. (2006a) at Vernon (Fig. 1), on the other hand, interpreted ≤12 km of extension, calling into question the magnitude of extension across the Okanagan Valley shear zone generally, and the presence of a major through-going detachment system.

Evidence for a Major Detachment

The presence of a major detachment and shear zone within the southern Okanagan Valley is supported by: (1) the metamorphic break observed across the Okanagan valley; (2) the localized zone of intense, Eocene, noncoaxial deformation recorded within the gneisses (i.e., the Okanagan Valley shear zone) as well as the strain gradient observed between rocks in the hanging wall and the Okanagan gneiss and Okanagan batholith in the footwall; and (3) the presence of contemporaneous Eocene cooling ages, felsic intrusions, and migmatization in the footwall, and coeval sedimentary and volcanic deposits in syntectonic hanging-wall half graben (Fig. 13).

Thermobarometry, combined with a lack of retrograde reaction rims around garnet porphyroblasts, indicates that the Okanagan gneiss was rapidly exhumed from ~20 km (Fig. 4) and cooled through 500 °C (the blocking temperature for Mn diffusion in garnet; Ganguly, 2002). Eocene peak pressure and depth estimates in the Okanagan gneiss are similar to those from coeval sillimanite-grade metapelites in the Kelowna area (Fig. 1; Bardoux, 1993) and the Grand Forks gneiss (Laberge and Pattison, 2007). In contrast, the hanging wall of the Okanagan Valley shear zone generally experienced no greater than greenschist-facies metamorphism in the Mesozoic, and negligible Eocene metamorphism; Eocene coals have vitrinite reflectance values comparable with burial to ≤3.5 km (Eyal et al., 2006).

Evidence for extensional deformation within the shear zone has been described in detail herein. In summary, evidence includes: (1) consistent top-down-to-the-west sense of shear indicators within the Okanagan gneiss and cataclastic rocks, (2) strongly prolate, noncoaxial strain fabrics including transposed gneissic foliation, sheath folds, and elongation lineation; (3) a pervasive, foliation-parallel mylonitic fabric; and (4) a strain gradient developed between the nondeformed Okanagan batholith and the Eocene sedimentary and volcanic rocks in the hanging wall. Similar evidence has been used to infer the presence of a major ductile shear zone and detachment along the length of the Okanagan Valley shear zone (Fig. 1; e.g., Bardoux, 1993; Kruckenberg et al., 2008), including in the Vernon area (Glombick et al., 2006a, 2006b), and along the margins of other gneiss domes within the Shuswap metamorphic complex (e.g., Parrish et al., 1988; Laberge and Pattison, 2007).

The most persuasive evidence for large-scale, rapid cooling in the Eocene facilitated by extension along the Okanagan Valley shear zone is the difference in cooling ages between the footwall and the hanging wall. Intrusive rocks in the hanging wall give Jurassic and Cretaceous cooling ages (White et al., 1968; Roddick et al., 1972; Medford, 1975; Fox et al., 1976; Parrish et al., 1988); therefore, the hanging wall has remained below 280 °C since the Mesozoic (~9 km depth using an elevated paleogeotherm of 30 °C/km). In contrast, the footwall consistently yields ca. 56–45 Ma cooling ages for both high- and low-temperature thermochronometers (Fig. 13; Baadsgaard et al., 1961; Ross, 1974; Medford, 1975; Wanless et al., 1978; Mathews, 1981; Stevens et al., 1982; Archibald et al., 1984; Armstrong et al., 1991; Bardoux, 1993; Kruckenberg et al., 2008; Toraman et al., 2011). Eocene high-temperature cooling ages (e.g., hornblende) are interpreted to record exhumation of hornblende through the 500 °C isotherm (≤10 km depth) from amphibolite-facies metamorphism and anatexis at ~20 km (Parrish et al., 1988; Johnson and Brown, 1996; Carr, 1992; Bardoux, 1993). Cooling between the zircon crystallization to Ar closure temperatures likely occurred within a few million years (Hansen and Goodge, 1988; Kruckenberg and Whitney, 2011). Exhumation and cooling were, therefore, contemporaneous with anatexis (e.g., Figs. 10, 11, and 13; Kruckenberg et al., 2008), syntectonic felsic intrusions (Figs. 12 and 13), post-tectonic felsic intrusions (48.6 ± 0.7 Ma; Bardoux, 1993), volcanism in the hanging wall (Church, 1985), and syntectonic supradetachment basin sedimentation (Wingate and Irving, 1994; Suydam and Gaylord, 1997).

Collectively, the data presented in this and previous studies suggest that the Okanagan gneiss was exhumed from at least 20 km depth to shallow levels in the crust (<3 km) during the Eocene (ca. 56–45 Ma). Similar geochronological and thermochronological data have been measured elsewhere in the Shuswap metamorphic complex and have been interpreted to result from rapid Eocene exhumation (e.g., Vanderhaeghe et al., 1999; Teyssier et al., 2005; Rey et al., 2009a).

Magnitude of Extension across the Okanagan Valley Shear Zone

Using the pre-exhumation depth established from geothermobarometry (6 ± 1 kbar, 17–23 km; Fig. 4) and the mean dip angle of the Okanagan Valley shear zone (15°; Fig. 2), we estimate a horizontal displacement of 64–89 km. We use the current dip of the foliation as a proxy for the average dip of the Okanagan Valley shear zone. Many studies demonstrate that low-angle detachments between footwall and hanging wall accommodate crustal extension (e.g., Davis and Lister, 1988; Livaccari et al., 1995; Chéry, 2001; Livaccari and Geissman, 2001; Chiaraluce et al., 2007; Phillips and Maikowski, 2011) without necessarily having evolved from high-angle normal faults in the hanging wall. Therefore, it is not necessary, nor

appropriate given our data, to assume that extension was accommodated exclusively, or in large part, along a now-deformed high-angle shear zone. Thus, we use the current average dip and accept that it will over- or underestimate the magnitude of extension if the Okanagan Valley shear zone has been reorientated since it was an active shear zone.

If the mobilization of low-viscosity melt-rich crust flow into culminations played a significant role, estimates of the magnitude of extension will be overestimated (Tirel et al., 2004; Rey et al., 2011); however, the small, volume of localized migmatite does not allow us to assess this quantitatively.

Our new estimates (64–89 km), arrived at through geometry and geothermobarometry, agree with those of Parkinson (1985) and Tempelman-Kluit and Parkinson (1986), who used pinning points between the Coryell syenite and alkaline volcanic rocks in the hanging wall. Furthermore, large-magnitude extension is expected given that the crust in the Shuswap metamorphic complex was thinned by 50% in the Eocene, from 50 to 60 km in the Paleocene (Brown et al., 1986; Gibson et al., 2008) to 32 km (Cook et al., 1988).

SUMMARY

Three lithological domains can be distinguished within the Okanagan gneiss, which include felsic orthogneiss, a mixed paragneiss and mafic orthogneiss domain, and a migmatite domain. New field observations augmented by new U-Pb zircon dates of the Okanagan gneiss and associated intrusions refine the relative and absolute timing of deformation within the southern Okanagan Valley shear zone. We constrain crustal exhumation from 20 km depth at 56–49 Ma, accommodated by 64–89 km of extension along the Okanagan Valley shear zone. Diverse lithologies and U-Pb zircon ages from the Okanagan gneiss record a range of geological events, including early to middle Mesozoic deposition of a sedimentary protolith, Jurassic and Cretaceous magmatism (and metamorphism), and Eocene migmatization, magmatism, and deformation related to exhumation. There is no evidence for a pre-Eocene fabric, nor evidence for a Paleoproterozoic protolith; therefore, we conclude that the Okanagan gneiss is not a piece of North American basement.

APPENDIX A

Electron Microprobe Methodology

Electron microprobe analyses were performed at the University of British Columbia using an automated four spectrometer Cameca SX-50 electron microprobe by the wavelength dispersive X-ray analysis method (WDX). Operating conditions were 20 kilovolts (kV) accelerating potential and a beam current of 10 nanoamperes (nA).The electron beam was rastered over a 3 by 3 μm area of the analyzed minerals. Counting times were up to 50 s or 40,000 accumulated counts on the main peaks with background count time normally on the order or 5–10 s, except for F and Cl at 30 s. X-ray lines were chosen to minimize or eliminate possible elemental interferences. Raw X-ray data were converted to elemental weight % via the Cameca PAP matrix correction program (Pouchou and Pichoir, 1984). For the elements considered, the following standards, X-ray lines, and mineral standards were used: grossular, Al K_α, TAP (Thallium Acid Pthalate); diopside, Mg K_α, TAP; grossular, Si K_α, TAP; diopside, Ca K_α, PET (Pentaerythirtol); rutile, Ti K_α, PET; synthetic chromite, Cr K_α, LIF (Lithium Fluoride); $MnTiO_3$, Mn K_α, LIF; synthetic fayalite, Fe K_α, LIF; orthoclase, K K_α, PET; phlogopite, F K_α, TAP; tugtupite, Cl K_α, PET; albite, Na K_α, TAP.

APPENDIX B

LA-ICP-MS Methodology

U-Pb dating of zircon by laser ablation–inductively coupled plasma–mass spectrometry (LA-ICP-MS) was conducted at Washington State University following the methods of Chang et al. (2006). A ThermoFinnigan Element2 single-collector, magnetic sector, double-focusing ICP-MS coupled with a New Wave Research Nd:YAG UV 213 nm laser was used. A laser spot size of 30 μm and a repetition rate of 10 Hz were used to ablate pits ~25 mm deep. He and Ar carrier gases delivered the sample aerosol to the plasma, and each analysis consisted of a blank analysis followed by 300 sweeps through masses 202, 204, 206, 207, 208, 232, 235, and 238, taking ~35 s.

Time-dependent interelement fractionation during the excavation of the laser pit was corrected using the intercept method (Kosler and Sylvester, 2003). The use of the intercept method for the correction of time-dependent interelement fractionation is predicated on the assumption of a linear increase in $^{206}Pb/^{238}U$ and $^{207}Pb/^{235}U$ ratios with time during a given laser-ablation analysis (Gaschnig et al., 2010). Numerous analyses yielded stable and reproducible $^{207}Pb/^{206}Pb$ ratios but U/Pb ratios with chaotic and nonlinear time-dependent trends, which renders their $^{206}Pb/^{238}U$ and $^{207}Pb/^{235}U$ intercepts and therefore $^{206}Pb/^{238}U$ and $^{207}Pb/^{235}U$ ages meaningless. This result is unlikely to represent the ablation from one age domain to another during the analysis because this should produce an analogous change in the $^{207}Pb/^{206}Pb$ ratio. The disrupted U/Pb could be the result of Pb loss or zircon recrystallization.

Time-independent (or static) fractionation was corrected by normalizing U/Pb and Pb/Pb ratios measured on unknown analyses with fractionation factors derived from analyzing standards. Total uncertainty for each laser analysis of an unknown is combined quadratically from the uncertainty in the measured isotope ratios of the unknown (uncertainties in the intercept or mean of the unknown analyses) and the uncertainty in the fractionation factors calculated from the measurement of standards.

At the beginning of each analytical session, two or three zircon standards (FC-1, Peixe, and occasionally R33) were analyzed multiple times until fractionation was stable. During a session, each standard was measured two to three times before and after a group of ~10 unknown analyses. Data reduction was performed separately using an Excel program with Visual Basic macros (Chang et al., 2006), where the count rates for blanks were calculated by averaging the signal intensities of 300 sweeps, with spikes more than twice the average filtered out. The blank was then subtracted from the corresponding sample analysis. The isotope ratios $^{206}Pb/^{238}U$ and $^{207}Pb/^{206}Pb$ were calculated for every sweep using the blank-corrected signal intensities. The ratios of 300 sweeps were plotted on time-series diagrams. For the $^{206}Pb/^{238}U$ measurements, a straight-line fit through the data was conducted by least squares regression, and points outside of the 95% confidence range (2σ) of the regression line were removed by an Excel macro. The intercept and standard error of the $^{206}Pb/^{238}U$ intercept were calculated using an Excel function. For the $^{207}Pb/^{206}Pb$ ratio, the in-run error is the standard error as calculated on the mean of the $^{207}Pb/^{206}Pb$ measurements because there is no time dependence in this ratio over the course of the analysis. Fractionation factors (FF) were determined on the basis of the ratio of the "true" $^{206}Pb/^{238}U$, $^{207}Pb/^{235}U$, and $^{207}Pb/^{206}Pb$ values for the standard to their measured values (FF = true ratio/measured ratio). Once the FF values for all three unknowns were found, they were applied to the unknowns in order to calculate the corrected ratios (corrected ratio = measured ratio × FF). Final ages and uncertainties were calculated using the corrected ratios and their associated uncertainties.

Although common Pb corrections for Mesozoic and younger zircon are typically very low (e.g., ~0.1 m.y. for Late Cretaceous zircon), common Pb corrections were applied where the $^{207}Pb/^{206}Pb$ age exceeded the $^{206}Pb/^{238}U$ age by more than the error on the $^{207}Pb/^{206}Pb$ age, but this is insignificant unless the $^{207}Pb/^{206}Pb$ age is several hundred million years greater than the $^{206}Pb/^{238}U$ age. Common Pb is typically not significant in LA-ICP-MS analyses, because it is concentrated in avoidable cracks and inclusions (Gaschnig et al., 2010). When it is not possible to avoid these areas, the influence of common Pb is easy to recognize on Tera-Wasserburg diagrams because analyses lie off the concordia line in the direction of common Pb on a steep linear trajectory that can be anchored at a reasonable $^{207}Pb/^{206}Pb$ common lead composition (*y*-intercept = 0.86 ± 0.06; DeGraaff-Surpless et al., 2002). Common Pb corrections were made on these analyses using the ^{207}Pb method (Williams, 1998).

SHRIMP Methodology

Sensitive high-resolution ion microprobe (SHRIMP) U-Pb isotopic analyses were carried out at the Geological Survey of Canada, Ottawa; analytical procedures followed those described by Stern (1997), with standards (z6266, Temora 2) and U-Pb calibration methods following Stern and Amelin (2003). Mount surfaces were evaporatively coated with 10 nm of high-purity Au. Analyses were conducted using an $^{16}O^-$ primary beam, projected onto the zircon at 10 kV. The sputtered area used for analysis was ~25 μm in diameter with a beam current of ~15 nA. SHRIMP pits were less than 1 μm deep (Stern, 1997). The count rates of 10 isotopes of Zr^+, U^+, Th^+, and Pb^+ in zircon were sequentially measured over six scans with a single electron multiplier and a pulse-counting system with

dead time of 27 ns. Off-line data processing was accomplished using customized in-house software (SQUID2). Due to a change in the primary beam conditions halfway through the analytical session, two U-Pb fractionation calibrations were required. The 1σ external errors of $^{206}Pb/^{238}U$ ratios reported in the data table (see GSA Data Repository DR3 [see footnote 1]) incorporate either a ±1.4% or a 1.13% error in calibrating the standard zircon (see Stern and Amelin, 2003). Analyses of a secondary zircon standard (Temora 2) were interspersed to verify the accuracy of the second U-Pb calibration. Using the calibration defined by the z6266 standard, the weighted mean $^{206}Pb/^{238}U$ age of eight SHRIMP analyses of Temora 2 zircon is 415.8 ± 3.4 Ma (95% confidence). The accepted $^{206}Pb/^{238}U$ age of Temora 2 is 416.5 ± 0.22 Ma, based on 21 isotope dilution fractions (Black et al., 2004). No fractionation correction was applied to the Pb-isotope data.

Unless otherwise stated, $^{206}Pb/^{238}U$ weighted mean ages were corrected for common Pb using the ^{207}Pb method. The common Pb correction utilized the measured $^{207}Pb/^{206}Pb$ and the Pb compositions of the surface Au coating of the grain mount (Au $^{207}Pb/^{206}Pb$ common Pb ratio is 0.895, error 0.1%; Stern, 1997). Analyses with ages older than 1000 Ma are reported as ^{204}Pb-corrected $^{207}Pb/^{206}Pb$ ages. Plots and calculations were carried out using IsoPlot 3.0 of Ludwig (2003).

ACKNOWLEDGMENTS

Funding was provided through Natural Sciences and Engineering Research Council of Canada grants held by Gibson and awards to Brown from Simon Fraser University, American Association of Petroleum Geologists, and Sigma Xi. We wish to thank Helena Kuikka, Megan Jamer, and Charles Knaack for help in the field and laboratory. Andrew Okulitch, Kirk Osadetz, and Jim Morin provided essential encouragement and local knowledge. Matti Raudsepp (University of British Columbia) advised us on electron microprobe use and access. Reviews by Jim Crowley, Seth Kruckenberg, Maurice Colpron, and Randy Parrish greatly improved the manuscript. We thank John Goodge for handling the manuscript.

REFERENCES CITED

Archibald, D.A., Krough, T.E., Armstrong, R.L., and Farrar, E., 1984, Geochronology and tectonic implications of magmatism and metamorphism, southern Kootenay arc and neighboring regions, southeastern British Columbia. Part II: Mid-Cretaceous to Eocene: Canadian Journal of Earth Sciences, v. 21, p. 567–583, doi:10.1139/e84-062.

Armstrong, R.L., 1988, Mesozoic and early Cenozoic magmatic evolution of the Canadian Cordillera, *in* Clark, S.P., Jr., Burchfiel, B.C., and Suppe, J., eds., Processes in Continental Lithospheric Deformation: Geological Society of America Special Paper 218, p. 55–91.

Armstrong, R.L., Parrish, R.R., van der Heyden, P., Scott, K., Runkle, D., and Brown, R.L., 1991, Early Proterozoic basement exposures in the southern Canadian Cordillera: Core gneiss of Frenchman Cap, Unit I of the Grand Forks Gneiss, and the Vaseaux Formation: Canadian Journal of Earth Sciences, v. 28, p. 1169–1201, doi:10.1139/e91-107.

Baadsgaard, H., Folinsbee, R.E., and Lipson, J., 1961, Potassium-argon dates of biotites from Cordilleran granites: Geological Society of America Bulletin, v. 72, p. 689–701, doi:10.1130/0016-7606(1961)72[689:PDOBFC]2.0.CO;2.

Bardoux, M., 1993, The Okanagan Valley Normal Fault from Penticton to Enderby, South-Central British Columbia [Ph.D. thesis]: Ottawa, Ontario, Carleton University, 292 p.

Bardoux, M., and Mareschal, J.-C., 1994, Extension in south-central British Columbia: Mechanical and thermal controls: Tectonophysics, v. 238, p. 451–470, doi:10.1016/0040-1951(94)90068-X.

Berman, R.G., 1991, Thermobarometry using multi-equilibrium calculations: A new technique, with petrological applications, *in* Gordon, T.M., and Martin, R.F., eds., Quantitative Methods in Petrology: An Issue in Honor of Hugh J. Greenwood: Canadian Mineralogist, v. 29, p. 833–855.

Berman, R.G., 2007, winTWQ (version 2.3): A Software Package for Performing Internally-Consistent Thermobarometric Calculations: Geological Survey of Canada Open-File 5462, ed. 2.34, 41 p.

Berman, R.G., and Aranovich, L.Y., 1996, Optimized standard state and solution properties of minerals: I. Calibration for olivine, orthopyroxene, cordierite, garnet, and ilmenite in the system FeO–MgO–CaO–Al_2O_3–TiO_2–SiO_2: Contributions to Mineralogy and Petrology, v. 126, p. 1–24, doi:10.1007/s004100050232.

Berman, R.G., Aranovich, L.Y., Rancourt, D.G., and Mercier, P.H.J., 2007, Reversed phase equilibrium constraints on the stability of Mg-Fe-Al biotite: The American Mineralogist, v. 92, no. 1, p. 139–150, doi:10.2138/am.2007.2051.

Black, L.P., Kamo, S.L., Allen, C.M., Davis, D.W., Aleinikoff, J.N., Valley, J.W., Mundil, R., Campbell, I.H., Korsh, R.J., Williams, I.S., and Foudoulis, C., 2004, Improved $^{206}Pb/^{238}U$ microprobe geochronology by monitoring of a trace-element–related matrix effect; SHRIMP, ID-TIMS, ELA-ICP-MS and oxygen isotope documentation for a series of zircon standards: Chemical Geology, v. 205, p. 115–140.

Bostock, H.S., 1941, Okanagan Falls: Geological Survey of Canada Map 627A, scale 1:63,360.

Breitsprecher, K., and Mortensen, J.K., 2004, BCAge 2004A–1—A database of isotopic age determinations for rock units from British Columbia: British Columbia Ministry of Energy and Mines, Geological Survey Open-File 2004-3 (Release 3.0), 7757 records.

Brown, R.L., and Gibson, H.D., 2006, An argument for channel flow in the southern Canadian Cordillera and comparison with Himalayan tectonics, *in* Law, R.R., Searle, M.P., and Godin, L., eds., Channel Flow, Ductile Extrusion and Exhumation in Continental Collision Zones: Geological Society of London Special Publication 268, p. 543–559.

Brown, R.L., Journeay, J.M., Lane, L.S., Murphy, D.C., and Rees, C.J., 1986, Obduction, backfolding and piggyback thrusting in the metamorphic hinterland of the southeastern Canadian Cordillera: Journal of Structural Geology, v. 8, p. 255–268, doi:10.1016/0191-8141(86)90047-7.

Brown, S.R., 2010, Geology and Geochronology of the Southern Okanagan Valley Shear Zone, Southern Canadian Cordillera, British Columbia [Ph.D. thesis]: Burnaby, British Columbia, Canada, Simon Fraser University, 320 p.

Carr, S.D., 1992, Tectonic setting and U-Pb geochronology of the Early Tertiary Ladybird leucogranite suite, Thor-Odin-Pinnacles area, southern Omineca Belt, British Columbia: Tectonics, v. 11, p. 258–278, doi:10.1029/91TC01644.

Chang, Z., Vervoort, J.D., McClelland, W.C., and Knaack, C., 2006, U-Pb dating of zircon by LA-ICP-MS: Geochemistry, Geophysics, Geosystems, Technical Brief 7, Q05009, p. 1–14.

Chery, J., 2001, Core complex mechanics: From the Gulf of Corinth to the Snake Range: Geology, v. 29, p. 439–442.

Chiaraluce, L., Chiarabba, C., Collettini, C., Piccinini, D., and Cocco, M., 2007, Architecture and mechanics of an active low-angle normal fault: Alto Tiberina Fault, northern Apennines, Italy: Journal of Geophysical Research, v. 112, B10310, doi:10310.11029/12007JB005015.

Christie, J.S., 1973, Geology of the Vaseaux Lake Area [Ph.D. thesis]: Vancouver, British Columbia, Canada, University of British Columbia, 136 p.

Church, B.N., 1973, Geology of the White Lake Basin British Columbia: Department of Mines and Petroleum Resources Bulletin 61, p. 3–141.

Church, B.N., 1985, Volcanology and Structure of Tertiary Outliers in south-central British Columbia: Geological Society of America Cordilleran Section Field Trip Guidebook, Vancouver, B.C., May, 1985 Meeting, Trip 5, 46 p.

Colpron, M., Price, R.A., Archibald, D.A., and Carmichael, D.M., 1996, Middle Jurassic exhumation along the western flank of the Selkirk fan structure: Thermobarometric and thermochronometric constraints from the Illecillewaet synclinorium, southeastern British Columbia: Geological Society of America Bulletin, v. 108, p. 1372–1392, doi:10.1130/0016-7606(1996)108<1372:MJEATW>2.3.CO;2.

Coney, P.J., 1980, Cordilleran metamorphic core complexes: An overview, *in* Crittenden, M.D., Coney, P.J., and Davis, G.H., eds., Cordilleran Metamorphic Core Complexes: Geological Society of America Memoir 153, p. 7–13.

Cook, F.A., 1995, The reflection Moho beneath the southern Canadian Cordillera: Canadian Journal of Earth Sciences, v. 32, p. 1520–1530, doi:10.1139/e95-124.

Cook, F.A., Green, A.G., Simony, P.S., Price, R.A., Parrish, R.R., Mikereit, B., Gordy, P.L., Brown, R.L., Coflin, K.C., and Patenaude, C., 1988, Lithoprobe seismic reflection structure of the southeastern Canadian Cordillera: Initial results: Tectonics, v. 7, p. 157–180, doi:10.1029/TC007i002p00157.

Cook, F.A., Varsek, J.L., Clowes, R.M., Kanasewich, E.R., Spencer, C.S., Parrish, R.R., Brown, R.L., Carr, S.D., Johnson, B.J., and Price, R.A., 1992, Lithoprobe crustal reflection cross section of the southern Canadian Cordillera: 1. Foreland thrust and fold belt to Fraser River Fault: Tectonics, v. 11, p. 12–35, doi:10.1029/91TC02332.

Corfu, F., Hanchar, J.M., Hoskin, P.W.O., and Kinny, P., 2003, Atlas of zircon textures, *in* Hanchar, J.H., and Hoskin, P.W.O., eds., Zircon: Mineralogical Society of America Reviews in Mineralogy and Geochemistry, v. 53, p. 469–500.

Crider, J.G., and Callahan, O.A., 2011, Persistently high geothermal gradient above the Okanogan detachment: Thermal weakening is a cause but not trigger of orogenic collapse: Geological Society of America Abstracts with Programs, v. 43, no. 5, p. 554.

Crowley, J.L., 1997, U-Pb geochronological constraints on the cover sequence of the Monashee complex, Canadian Cordillera: Paleoproterozoic deposition on basement: Canadian Journal of Earth Sciences, v. 34, p. 1008–1022, doi:10.1139/e17-083.

Crowley, J.L., 1999, U-Pb geochronologic constraints on Paleoproterozoic tectonism in the Monashee complex, Canadian Cordillera: Elucidating an overprinted geologic history: Geological Society of America Bulletin, v. 111, p. 560–577, doi:10.1130/0016-7606(1999)111<0560:UPGCOP>2.3.CO;2.

Crowley, J.L., Brown, R.L., and Parrish, R.R., 2001, Diachronous deformation and a strain gradient beneath the Selkirk allochthon, northern Monashee complex, southeastern Canadian Cordillera: Journal of Structural Geology, v. 23, p. 1103–1121, doi:10.1016/S0191-8141(00)00179-6.

Crowley, J.L., Brown, R.L., Gervais, F., and Gibson, H.D., 2008, Assessing inheritance of zircon and monazite in granitic rocks from the Monashee complex, Canadian Cordillera: Journal of Petrology, v. 49, p. 1915–1929, doi:10.1093/petrology/egn047.

Cui, Y., and Erdmer, P., 2009, Geological Map of British Columbia: British Columbia Ministry of Energy, Mines and Petroleum Resources, Geoscience Map 2009-1A, scale 1:2,000,000, 1 sheet.

Davis, G.A., and Lister, G.S., 1988, Detachment faulting in continental extension: Perspectives from the south-western U.S. cordillera, *in* Clark, S.P., Jr., Burchfiel, B.C., and Suppe, J., eds., Processes in Continental Lithospheric Deformation: Geological Society of America Special Paper 218, p. 133–159.

Davis, G.H., 1983, Shear-zone model for the origin of metamorphic core complexes: Geology, v. 11, p. 342–347, doi:10.1130/0091-7613(1983)11<342:SMFTOO>2.0.CO;2.

DeGraaff-Surpless, K., Graham, S.A., Wooden, J.L., and McWilliams, M.O., 2002, Detrital zircon provenance analysis of the Great Valley Group, California: Evolution of an arc-forearc system: Geological Society of America Bulletin, v. 114, p. 1564–1580, doi:10.1130/0016-7606(2002)114<1564:DZPAOT>2.0.CO;2.

Diakow, L.J., and Barrios, A., 2009, Geology and mineral occurrences of the Mid-Cretaceous Spences Bridge Group near Merritt, southern British Columbia: British Columbia Geological Survey Geological Fieldwork 2008 Paper 2009-1, p. 63–79.

Ewing, T.E., 1980, Paleogene tectonic evolution of the Pacific Northwest: The Journal of Geology, v. 88, p. 619–638, doi:10.1086/628551.

Ewing, T.E., 1981, Regional stratigraphy and structural setting of the Kamloops Group, south-central British Columbia: Canadian Journal of Earth Sciences, v. 18, p. 1464–1477, doi:10.1139/e81-137.

Eyal, Y., Feinstein, S. and Osadetz, K., 2006, Brittle aspects of Early Tertiary extension in the Canadian Cordillera: Geophysical Research Abstracts, v. 8, abstract 04613, SRef-ID: 1607–7962/gra/EGU06-A-04613.

Ferry, J.M., and Spear, F.S., 1978, Experimental calibration of the partitioning of Fe and Mg between biotite and garnet: Contributions to Mineralogy and Petrology, v. 66, p. 113–117, doi:10.1007/BF00372150.

Fox, K.F., Jr., Rinehart, C.D., Engels, J.C., and Stern, T.W., 1976, Age of emplacement of the Okanogan gneiss dome, north-central Washington: Geological Society of America Bulletin, v. 87, p. 1217–1224, doi:10.1130/0016-7606(1976)87<1217:AOEOTO>2.0.CO;2.

Fuhrman, M.L., and Lindsley, D.H., 1988, Ternary-feldspar modelling and thermometry: American Mineralogist, v. 73, p. 201–215.

Ganguly, J., 2002, Diffusion kinetics in minerals: Principles and applications to tectono-metamorphic processes, *in* Gramaccioli, C.M., ed., Energy Modelling in Minerals: European Mineralogical Union Notes in Mineralogy, v. 4, p. 271–309.

Gaschnig, R.M., Vervoort, J.D., Lewis, R., and McClelland, W., 2010, Migrating magmatism in the northern US Cordillera: In situ U-Pb geochronology of the Idaho batholith: Contributions to Mineralogy and Petrology, v. 159, p. 863–883, doi:10.1007/s00410-009-0459-5.

Gervais, F., and Brown, R.L., 2011, Testing modes of exhumation in collisional orogens: Synconvergent channel flow in the southeastern Canadian Cordillera: Lithosphere, v. 3, no. 1, p. 55–75, doi:10.1130/L98.1.

Gervais, F., Brown, R.L., and Crowley, J.L., 2010, Tectonic implications for a Cordilleran orogenic base in the Frenchman Cap Dome, southeastern Canadian Cordillera: Journal of Structural Geology, v. 32, p. 941–959, doi:10.1016/j.jsg.2010.05.006.

Ghosh, D.K., 1995a, U-Pb geochronology of Jurassic to Early Tertiary granitic intrusives from the Nelson-Castlegar area, southeastern British Columbia, Canada: Canadian Journal of Earth Sciences, v. 32, p. 1668–1680, doi:10.1139/e95-132.

Ghosh, D.K., 1995b, Nd-Sr isotopic constraints on the interactions of the Intermontane superterrane with the western edge of North America in the southern Canadian Cordillera: Canadian Journal of Earth Sciences, v. 32, p. 1740–1758, doi:10.1139/e95-136.

Gibson, H.D., Brown, R.L., and Parrish, R.R., 1999, Deformation-induced inverted metamorphic field gradients, an example from southeastern Canadian Cordillera: Journal of Structural Geology, v. 21, no. 7, p. 751–767, doi:10.1016/S0191-8141(99)00051-6.

Gibson, H.D., Brown, R.L., and Carr, S.D., 2008, Tectonic evolution of the Selkirk fan, southeastern Canadian Cordillera: A composite Middle Jurassic–Cretaceous orogenic structure: Tectonics, v. 27, doi:10.1029/2007TC002160.

Glombick, P., Thompson, R., Erdmer, P., and Daughtry, K., 2006a, A reappraisal of the tectonic significance of Early Tertiary low-angle shear zones exposed in the Vernon map area (82 L), Shuswap metamorphic complex, southeastern Canadian Cordillera: Canadian Journal of Earth Sciences, v. 43, p. 245–268, doi:10.1139/e05-101.

Glombick, P., Thompson, R., Erdmer, P., Heaman, L., Friedman, M., Villeneuve, M., and Daughtry, K., 2006b, U-Pb constraints on the thermotectonic evolution of the Vernon antiform and the age of the Aberdeen gneiss complex, southeastern Canadian Cordillera: Canadian Journal of Earth Sciences, v. 43, p. 213–244, doi:10.1139/e05-096.

Goodge, J.W., and Hansen, V.L., 1983, Petrology and structure of rocks in the southwest portion of Okanogan Dome, north-central Washington: Northwest Geology, v. 12, p. 13–24.

Gordon, S.M., Whitney, D.L., Teyssier, C., Grove, M., and Dunlap, W.J., 2008, Timescales of migmatization, melt crystallization, and cooling in a Cordilleran gneiss dome: Valhalla complex, southeastern British Columbia: Tectonics, v. 27, TC4010, doi:10.1029/2007TC002103.

Hansen, V.L., and Goodge, J.W., 1988, Metamorphism, structural petrology, and regional evolution of the Okanogan complex, northeastern Washington, *in* Metamorphism and Crustal Evolution of the Western United States, Rubey Colloquium Volume 7, p. 233–270.

Harrison, T.M., Duncan, I., and McDougall, I., 1985, Diffusion of ^{40}Ar in biotite: Temperature, pressure and compositional effects: Geochimica et Cosmochimica Acta, v. 49, p. 2461–2468, doi:10.1016/0016-7037(85)90246-7.

Hinchey, A., and Carr, S.D., 2006, The S-type Ladybird leucogranite suite of southeastern British Columbia: Geochemical and isotopic evidence for a genetic link with migmatite formation in the North American basement gneisses of the Monashee complex: Lithos, v. 90, p. 223–248, doi:10.1016/j.lithos.2006.03.003.

Hinchey, A.M., Carr, S.D., McNeill, P.D., and Rayner, N., 2006, Paleocene-Eocene high-grade metamorphism, anatexis and deformation in Thor–Odin dome, Monashee complex, southeastern British Columbia: Canadian Journal of Earth Sciences, v. 43, p. 1341–1365.

Hoisch, T.D., 1990, Empirical calibration of six geobarometers for the mineral assemblage quartz + muscovite + biotite + plagioclase + garnet: Contributions to Mineralogy and Petrology, v. 104, p. 225–234, doi:10.1007/BF00306445.

Hoisch, T.D., 1991, Equilibria within the mineral assemblage quartz + muscovite + biotite + garnet + plagioclase, and implications for the mixing properties of octahedrally-coordinated cations in muscovite and biotite: Contributions to Mineralogy and Petrology, v. 108, p. 43–54, doi:10.1007/BF00307325.

Holder, R.W., and McCarley Holder, G.A., 1988, The Colville batholith: Tertiary plutonism in northeast Washington associated with graben and core-complex (gneiss dome) formation: Geological Society of America Bulletin, v. 100, p. 1971–1980, doi:10.1130/0016-7606(1988)100<1971:TCBTPI>2.3.CO;2.

Hoskin, P.W.O., and Schaltegger, U., 2003, The composition of zircon and igneous and metamorphic petrogenesis, *in* Hanchar, J.H., and Hoskin, P.W.O., eds., Zircon: Mineralogical Society of America Reviews in Mineralogy and Geochemistry, v. 53, p. 27–62.

Hurlow, H.A., and Nelson, B.K., 1993, U-Pb zircon and monazite ages for the Okanogan Range batholiths, Washington: Implications for the magmatic and tectonic evolution of the southern Canadian and northern United States Cordillera: Geological Society of America Bulletin, v. 105, p. 231–240, doi:10.1130/0016-7606(1993)105<0231:UPZAMA>2.3.CO;2.

Irving, E., and Thorkelson, D.J., 1990, On determining paleohorizontal and latitudinal shifts: Paleomagnetism of Spences Bridge Group, British Columbia: Journal of Geophysical Research, v. 95, p. 19,213–19,234, doi:10.1029/JB095iB12p19213.

Irving, E., Thorkelson, D.J., Wheadon, P.M., and Enkin, R.J., 1995, Paleomagnetic of the Spences Group and northward displacements of the Intermontane Belt, British Columbia: A second look: Journal of Geophysical Research, v. 100, p. 6057–6071, doi:10.1029/94JB03012.

Johnson, B., 1994, Structure and Tectonic Setting of the Okanagan Valley Fault System in the Shuswap Lake Area, Southern British Columbia [Ph.D. thesis]: Ottawa, Ontario, Canada, Carleton University, 266 p.

Johnson, B., 2006, Extensional shear zones, granitic melts, and linkage of overstepping normal faults bounding the Shuswap metamorphic core complex, British Columbia: Geological Society of America Bulletin, v. 118, p. 366–382, doi:10.1130/B25800.1.

Johnson, B., and Brown, R., 1996, Crustal structure and Early Tertiary extensional tectonics of the Omineca belt at 51°N latitude, southern Canadian Cordillera: Canadian Journal of Earth Sciences, v. 33, p. 1596–1611, doi:10.1139/e96-121.

Kosler, J., Sylvester, P.J., 2003, Present trends and the future of zircon in geochronology: Laser ablation ICPMS, *in* Hanchar, J.M., and Hoskin, P.W.O., eds., Zircon: Reviews in Mineralogy and Geochemistry, v. 53, p. 243–275.

Kruckenberg, S.C., and Whitney, D.L., 2011, Metamorphic evolution of sapphirine- and orthoamphibole-cordierite–bearing gneiss, Okanogan Dome, Washington, USA: Journal of Metamorphic Geology, v. 29, p. 425–449, doi:10.1111/j.1525-1314.2010.00926.x.

Kruckenberg, S.C., Whitney, D.L., Teyssier, C., Fanning, C.M., and Dunlap, W.J., 2008, Paleocene-Eocene migmatite crystallization, extension, and exhumation in the hinterland of the northern Cordillera: Okanogan Dome, Washington, USA: Geological Society of America Bulletin, v. 120, p. 912–929, doi:10.1130/B26153.1.

Laberge, J.D., and Pattison, D.R.M., 2007, Geology of the western margin of the Grand Forks complex, southern British Columbia: High-grade Cretaceous metamorphism followed by Early Tertiary extension on the Granby fault: Canadian Journal of Earth Sciences, v. 44, p. 199–228, doi:10.1139/e06-101.

Leech, G.B., Lowdon, J.A., Stockwell, C.H., and Wanless, R.K., 1963, Age Determinations and Geological Studies: Geological Survey of Canada Paper 63-17, 140 p.

Livaccari, R.F., and Geissman, J.W., 2001, Large-magnitude extension along metamorphic core complexes of western Arizona and southeastern California: Evaluation with paleomagnetism: Tectonics, v. 20, p. 625–648, doi:10.1029/2000TC001244.

Livaccari, R.F., Geissman, J.W., and Reynolds, S.J., 1995, Large-magnitude extensional deformation in the South Mountains metamorphic core complex, Arizona: Evaluation with paleomagnetism: Geological Society of America Bulletin, v. 107, p. 877–894, doi:10.1130/0016-7606(1995)107<0877:LMEDIT>2.3.CO;2.

Ludwig, K.R., 2003, User's Manual for Isoplot/Ex rev. 3.00: A Geochronological Toolkit for Microsoft Excel: Berkeley Geochronology Center Special Publication 4, 70 p.

Massey, N.W.D., MacIntyre, D.G., Desjardins, P.J., and Cooney, R.T., 2005, Digital Geology Map of British Columbia: Whole Province: British Columbia Ministry of Energy and Mines GeoFile 2005-1, scale 1:2,000,000.

Mathews, W., 1981, Early Cenozoic resetting of potassium-argon dates and geothermal history of north Okanagan area, British Columbia: Canadian Journal of Earth Sciences, v. 18, p. 1310–1319, doi:10.1139/e81-121.

McClaughry, J.D., and Gaylord, D.R., 2005, Middle Eocene sedimentary and volcanic infilling of an evolving supradetachment basin: White Lake Basin, south-central British Columbia: Canadian Journal of Earth Sciences, v. 42, p. 49–66, doi:10.1139/e04-105.

Medford, G.A., 1975, K-Ar and fission track geochronometry of an Eocene thermal event in the Kettle River (west half) map area, southern British Columbia: Canadian Journal of Earth Sciences, v. 12, p. 836–843, doi:10.1139/e75-072.

Monger, J.W.H., Price, R.A., and Tempelman-Kluit, D.J., 1982, Tectonic accretion and the origin of the two major metamorphic and plutonic welts in the Canadian Cordillera: Geology, v. 10, p. 70–75, doi:10.1130/0091-7613(1982)10<70:TAATOO>2.0.CO;2.

Monger, J.W.H., Wheeler, J.O., Tipper, H.W., Gabrielse, H., Harms, T., Struik, L.C., Campbell, R.B., Dodds, C.J., Gehrels, G.E., and O'Brien, J., 1991, Upper Devonian to Middle Jurassic assemblages, *in* Gabrielse, H., and Yorath, C.J., eds., Geology of the Cordilleran Orogeny in Canada: Geological Survey of Canada, Geology of Canada, Series 4, p. 281–317 (also Geological Survey of America, The Geology of North America, v. G-2).

Morin, J.A., 1989, Drilling Report on the Gold Property, Osoyoos Mining Division, B.C., N.T.S. 82E–6W Latitude: 49°17′N, Longitude: 119°20′W BCGS: British Columbia Ministry of Energy, Mines and Petroleum Resources, Report 18892, 278 p.

Murphy, D.C., van der Heyden, P., Parrish, R.R., Klepacki, D.W., McMillan, W., Struik, L.C., and Gabites, J., 1995, New geochronological constraints on Jurassic deformation of the western edge of North America, southeastern Canadian Cordillera, *in* Miller, D.M., and Busby, C., eds., Jurassic Magmatism and Tectonics of the North American Cordillera: Geological Society of America Special Paper 299, p. 159–171.

Okulitch, A.V., 1973, Age and correlation of the Kobau Group, Mount Kobau, British Columbia: Canadian Journal of Earth Sciences, v. 10, p. 1508–1518, doi:10.1139/e73-143.

Okulitch, A.V., 1979, Geology and Mineral Occurrences of the Thompson-Shuswap-Okanagan Region, South-Central British Columbia: Geological Survey of Canada Open-File 637, scale 1:250,000, 1 sheet.

Okulitch, A.V., 1984, The role of the Shuswap metamorphic complex in Cordilleran tectonism: A review: Canadian Journal of Earth Sciences, v. 21, p. 1171–1193, doi:10.1139/e84-123.

Parkinson, D.L., 1985, U-Pb Geochronology and Regional Geology of the Southern Okanagan Valley, British Columbia: The Western Boundary of a Metamorphic Core Complex [M.S. thesis]: Vancouver, British Columbia, Canada, University of British Columbia, 149 p.

Parkinson, D.L., 1991, Age and isotopic character of Early Proterozoic basement gneisses in the southern Monashee complex, southeastern British Columbia: Canadian Journal of Earth Sciences, v. 28, p. 1159–1168, doi:10.1139/e91-106.

Parrish, R.R., 1995, Thermal evolution of the southeastern Canadian Cordillera: Canadian Journal of Earth Sciences, v. 32, p. 1618–1642, doi:10.1139/e95-130.

Parrish, R.R., Carr, S.D., and Parkinson, D.L., 1988, Eocene extensional tectonics and geochronology of the southern Omineca Belt, British Columbia and Washington: Tectonics, v. 7, p. 181–212, doi:10.1029/TC007i002p00181.

Phillips, F.M., and Majkowski, L., 2011, The role of low-angle normal faulting in active tectonics of the northern Owens Valley, California: Lithosphere, v. 3, p. 22–36, doi:10.1130/L73.1.

Pouchou, L.J., and Pichoir, F., 1984, New model quantitative x-ray microanalysis, 1. Application to the analysis of homogeneous samples: La Recherche Aérospatiale, v. 3, p. 13–38.

Reesor, J.E., and Moore, J.M.J., 1971, Petrology and Structure of Thor-Odin Gneiss Dome, Shuswap Metamorphic Complex: Geological Survey of Canada Bulletin 195, scale 1:50,000.

Rey, P., Teyssier, C., and Whitney, D.L., 2009a, Extension rates, crustal melting, and core complex dynamics: Geology, v. 37, p. 391–394, doi:10.1130/G25460A.1.

Rey, P., Teyssier, C., Kruckenberg, S., and Whitney, D.L., 2011, Viscous collision in channel explains double domes in metamorphic core complexes: Geology, v. 39, p. 387-390.

Reynolds, S.J., and Lister, G.S., 1990, Folding of mylonitic zones in Cordilleran metamorphic core complexes: Evidence from near the mylonitic front: Geology, v. 18, p. 216–219, doi:10.1130/0091-7613(1990)018<0216:FOMZIC>2.3.CO;2.

Roddick, C., Farrar, E., and Procyshyn, E.L., 1972, Potassium-argon ages of igneous rocks from the area near Hedley, southern British Columbia: Canadian Journal of Earth Sciences, v. 9, p. 1632–1639, doi:10.1139/e72-144.

Ross, J.V., 1974, A Tertiary thermal event in south-central British Columbia: Canadian Journal of Earth Sciences, v. 11, p. 1116–1122, doi:10.1139/e74-106.

Rubatto, D., and Gebauer, D., 2000, Use of cathodoluminescence for U-Pb zircon dating by ion microprobe: some examples from the Western Alps, *in* Pagel, M., Barbin, V., and Blanc, P., eds., Cathodoluminescence in Geosciences: Berlin, Ohnenstetter, Springer, p. 373–400.

Ryan, D., 1973, Structural Geology and Rb/Sr Geochronology of the Anarchist Mountain Area, South-Central British Columbia [Ph.D. thesis]: Vancouver, British Columbia, Canada, The University of British Columbia, 256 p.

Sawyer, E.W., 2008, Atlas of Migmatites: Canadian Mineralogist Special Publication 9, 371 p.

Sawyer, E.W., Cesare, B., and Brown, M., 2011, When the continental crust melts: Elements, v. 7, no. 4, p. 229–234, doi:10.2113/gselements.7.4.229.

Sinclair, A.J., Moore, D., and Reinsbakken, A., 1984, Geology of Gypo quartz vein, Oliver, British Columbia (82E/4): British Columbia Ministry of Energy, Mines and Petroleum Resources, Geological Fieldwork 1983, Paper 1984-1, p. 246–247.

Souther, J.G., 1991, Volcanic regimes, *in* Gabrielse, H., and Yorath, C.J., eds., Geology of the Cordilleran Orogeny in Canada: Geological Survey of Canada, Geology of Canada, Series 4, p. 457–490 (also Geological Society of America, The Geology of North America, v. G-2).

Spalla, M.I., Zanoni, D., Williams, P.F., and Gosso, G., 2011, Deciphering cryptic *P-T-d-t* histories in the western Thor-Odin Dome, Monashee Mountains, Canadian Cordillera: A key to unraveling pre-Cordilleran tectonic signatures: Journal of Structural Geology, v. 33, p. 399–421, doi:10.1016/j.jsg.2010.11.014.

Stern, R.A., 1997, The GSC sensitive high resolution ion microprobe (SHRIMP): Analytical techniques of zircon U-Th-Pb age determinations and performance evaluation: Geological Survey of Canada, Current Research 1997-F, Radiogenic Age and Isotopic Studies Report 10, p. 1–31.

Stern, R.A., and Amelin, Y., 2003, Assessment of errors in SIMS zircon U-Pb geochronology using a natural zircon standard and NIST SRM 610 glass: Chemical Geology, v. 197, p. 111–142, doi:10.1016/S0009-2541(02)00320-0.

Stevens, R.D., DeLabio, R.N., and Lachance, G.R., 1982, Age Determination and Geologic Studies: K-Ar Isotopic Ages: Geological Survey of Canada Report 16, Paper 82-2, 56 p.

Suydam, J.D., and Gaylord, D.R., 1997, Toroda Creek half graben, northeast Washington: Late-stage sedimentary infilling of a synextensional basin: Geological Society of America Bulletin, v. 109, p. 1333–1348, doi:10.1130/0016-7606(1997)109<1333:TCHGNW>2.3.CO;2.

Tempelman-Kluit, D., 1989, Geology, Penticton, British Columbia: Geological Survey of Canada Map 1736A, scale 1:250,000, 1 sheet.

Tempelman-Kluit, D., and Parkinson, D., 1986, Extension across the Eocene Okanagan crustal shear in southern British Columbia: Geology, v. 14, p. 318–321, doi:10.1130/0091-7613(1986)14<318:EATEOC>2.0.CO;2.

Teyssier, C., Ferre, E., Whitney, D.L., Norlander, B., Vanderhaeghe, O., and Parkinson, D., 2005, Flow of partially molten crust and origin of detachments during collapse of the Cordilleran orogen, *in* Bruhn, D., and Burlini, L., eds., High-Strain Zones: Structure and Physical Properties: Geological Society of London Special Publication 245, p. 39–64.

Thorkelson, D.J., 1989, Eocene sedimentation and volcanism in the Fig Lake graben, southwestern British Columbia: Canadian Journal of Earth Sciences, v. 26, p. 1368–1373, doi:10.1139/e89-116.

Tirel, C., Brun, J.-P., and Burov, E., 2004, Thermomechanical modeling of extensional gneiss domes, *in* Whitney, D.L., et al., eds., Gneiss Domes in Orogeny: Geological Society of America Special Paper 380, p. 67–78.

Toraman, E., Fayon, A., Whitney, D.L., Teyssier, C., Reiners, P.W., Thomson, S.N., and Kruckenberg, S.C., 2011, Apatite-zircon U-Th/He and fission-track dating of the Okanogan Dome exhumation (Washington, USA): Geological Society of America Abstracts with Programs, v. 43, no. 5, p. 654.

Vanderhaeghe, O., Teyssier, C., and Wysoczanski, R., 1999, Structural and geochronological constraints on the role of partial melting during the formation of the Shuswap metamorphic core complex at the latitude of the Thor-Odin Dome, British Columbia: Canadian Journal of Earth Sciences, v. 36, p. 917–943, doi:10.1139/e99-023.

Wanless, R.K., and Reesor, J.E., 1975, Precambrian zircon age of orthogneiss in the Shuswap metamorphic complex, British Columbia: Canadian Journal of Earth Sciences, v. 12, p. 326–332, doi:10.1139/e75-028.

Wanless, R.K., Stevens, R.D., Lachance, G.R., and Delabio, R.N., 1978, Age Determinations and Geological Studies—K-Ar Isotopic Ages: Geological Survey of Canada Report 13, Paper 77-2, 60 p.

Wheeler, J.O., 1965, Big Bend Map-Area, 82/M East-Half, British Columbia: Geological Survey of Canada Paper 64-32, 37 p.

Wheeler, J.O., and McFeely, P. (compilers), 1991, Tectonic Assemblage Map of the Canadian Cordillera and Adjacent Parts of the United States of America: Geological Survey of Canada Map 1712A, scale 1:2,000,000.

White, W.H., Harakal, J.E., and Carter, N.C., 1968, Potassium-argon ages of some ore deposits in British Columbia: Canadian Institute of Mining and Metallurgy Bulletin, v. 61, p. 1326–1334.

Williams, I.S., 1998, U-Th-Pb geochronology by ion microprobe, *in* McKibben, M.A., Shanks W.C., III, and Ridley, W.I., eds., Applications of Microanalytical Techniques to Understanding Mineralizing Processes: Reviews in Economic Geology, v. 7, p. 1–35.

Wingate, W.T.D., and Irving, E., 1994, Extension in high-grade terranes of the southern Omineca Belt, British Columbia: Evidence from paleomagnetism: Tectonics, v. 13, p. 686–711, doi:10.1029/93TC03490.

Winter, J.D., 2010, Principles of Igneous and Metamorphic Petrology 2nd Edition: Upper Saddle River, New Jersey, Prentice-Hall Inc.,702 p.

Woodsworth, G.J., Anderson, R.G., and Armstrong, R.L., 1991, Plutonic regimes, *in* Gabrielse, H., and Yorath, C.J., eds., Geology of the Cordilleran Orogen in Canada: Geological Survey of Canada, Geology of Canada Series 4 (also Geological Society of America, The Geology of North America, v. G-2), p. 491–531.

MANUSCRIPT RECEIVED 17 JANUARY 2012
REVISED MANUSCRIPT RECEIVED 27 APRIL 2012
MANUSCRIPT ACCEPTED 4 MAY 2012

Printed in the USA